cSINGV v1.0: Development and evaluation of a 1.5 km coupled atmosphere-ocean-wave modelling system for the Western Maritime Continent

Rajesh Kumar[1], Claudio Sanchez[2], Juan Manuel Castillo[2], Jian-Guo Li[2], Bijoy Thompson[3], Pratiman Patel[1], Alvin Ng[4], Kaushik Sasmal[3], Kalli Furtado[1], Hailin Yan[1], Liu Jianyu[1], and Hugh Zhang[1]

[1]Centre for Climate Research Singapore, Meteorological Service Singapore, 537054, Singapore
[2]Met Office, Exeter, EX1 3PB, United Kingdom
[3] Technology Centre for Offshore and Marine Singapore, 12 Prince George's Pk, 118411, Singapore
[4] Department of Mathematics, National University of Singapore, Singapore 119222, Singapore

Correspondence to: Rajesh Kumar (rajesh_kumar@nea.gov.sg)

Abstract. This study presents cSINGV v1.0, a high-resolution (1.5 km) regional coupled atmosphere–ocean–wave modelling system developed for the Western Maritime Continent (WMC), a region characterised by complex coastlines, shallow seas, and strong air–sea interactions. The system integrates a convection-permitting atmospheric model (SINGV) with newly configured ocean (NEMO) and wave (WAVEWATCH III) components within a unified coupling framework based on the Regional Coupled Suite and OASIS3-MCT coupler. Its primary contribution is the development of a fully coupled system that enables two-way interactions between atmosphere, ocean, and waves at kilometre scale. Before coupling, the ocean and wave components are configured in standalone mode for the WMC.

The model is evaluated using a six-month simulation (January–June 2019) against multiple observational and reanalysis datasets. The ocean and wave components show good agreement with reference datasets, with sea surface temperature errors generally below 0.5 °C and significant wave height errors around 0.2 m. This agreement is maintained in the fully coupled configuration. The influence of coupling is assessed by comparing the coupled and uncoupled atmospheric configurations. Results show that coupling improves the spatial organisation of precipitation, the diurnal cycle over the ocean, and the offshore propagation of convection, while differences in near-surface atmospheric variables remain modest. Process-based analysis indicates that these improvements are primarily linked to enhanced latent heat flux driven by thermodynamic air–sea feedbacks associated with sea surface temperature variability. Case studies of individual Sumatra squall events further suggest that coupling may influence the organisation and persistence of eastward-propagating convection. The magnitude of this influence appears to depend on the dominant convective regime, although a larger sample of events is needed to confirm this dependence. Overall, cSINGV provides a physically consistent framework for representing coupled processes in the WMC and a useful platform for investigating air–sea–wave interactions at convection-permitting scales.

1 Introduction

The Western Maritime Continent (WMC; Fig. 1) is characterised by complex topography, warm and predominantly shallow seas, and strong air–sea interactions (Neale and Slingo, 2003). Located between the Indian and Pacific Oceans, the region lies within the active propagation zones of the Madden–Julian Oscillation (MJO), the Intertropical Convergence Zone (ITCZ), and the boreal summer and winter monsoons, and consequently experiences some of the highest precipitation rates globally (Zhang, 2005; Yamanaka, 2016; Jiang and Li, 2018; Karlowska et al., 2024a). These rainfall patterns are driven by deep convection, sea-breeze convergence, and large-scale circulations such as the Walker and Hadley cells (Stone and Chervin, 1984; Kim et al., 2020). In addition, rainfall over the WMC is governed by interactions across multiple temporal and spatial scales, including interannual variability associated with ENSO, intraseasonal variability linked to the MJO, and synoptic-scale equatorial waves, together with local processes such as the diurnal cycle and topography (Peatman et al., 2014; Birch et al., 2016; Wei et al., 2020; Peatman et al., 2021; Senior et al., 2025). The diurnal cycle is a dominant feature of convection over the WMC, with thunderstorms typically developing over land in the afternoon and propagating offshore overnight (Mori et al., 2004; Yokoi et al., 2017; Peatman et al., 2025). Accurately representing these multiscale interactions remains a major challenge for numerical models, particularly given the strong coupling between the atmosphere and ocean in the region (Jiang et al., 2020, Xue et al., 2020 and references therein).

Air–sea interactions provide a key pathway linking these multiscale processes in the WMC, with sea surface temperature (SST) playing a central role in modulating atmospheric convection, surface fluxes, and boundary-layer processes (DeMott et al., 2015; Yoneyama and Zhang, 2020; Savarin and Chen, 2022; Karlowska et al., 2024a). Observations show that diurnal SST variability can significantly influence intraseasonal variability and surface turbulent fluxes, thereby affecting atmospheric dynamics (Ruppert and Johnson, 2015; Yan et al., 2021; Itterly et al., 2021). Despite this, atmosphere-only models typically prescribe SST as a fixed lower boundary, preventing realistic ocean–atmosphere feedbacks and often leading to biases in surface fluxes, SST variability, and convective organisation (e.g., Lau and Nath, 2003). Even small SST errors can substantially alter the timing and spatial distribution of precipitation (Dipankar et al., 2019), highlighting the importance of resolving SST variability for accurate prediction over the WMC. Similarly, ocean-only models rely on prescribed surface fluxes, limiting the ocean's dynamical response to atmospheric forcing (Bonino et al., 2022). Coupled atmosphere–ocean models overcome these constraints by enabling two-way interactions, improving SST and atmospheric simulations, particularly when high-frequency coupling is used (Wei et al., 2014; Seo et al., 2014; Zhao and Nasuno, 2020; Lan et al., 2024). Previous efforts have also demonstrated the feasibility and benefits of regional coupled atmosphere–ocean modelling over the Maritime Continent. For example, Thompson et al. (2021) describe the development of a kilometre-scale (~4.5 km) coupled prediction system based on the Met Office Unified Model and NEMO. Their results demonstrate that the coupled system provides realistic simulations

of SST, sea surface height (SSH), and subsurface ocean structure when evaluated against observations. These studies highlight the capability of regional coupled systems to improve ocean state representation in the Maritime Continent.

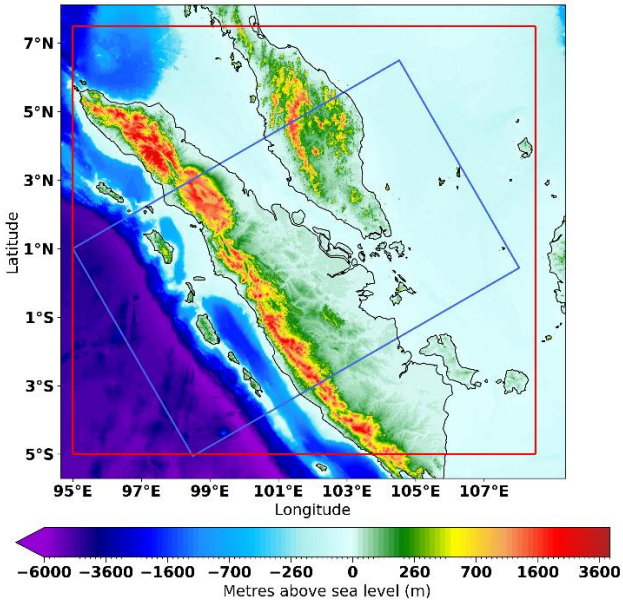


Figure 1: Ocean bathymetry and land orography over the Western Maritime Continent domain used in the cSINGV modelling system. The red box indicates the domain used for model evaluation in this study. The rotated blue box is used for the Sumatra Squall case study.

In addition to SST, ocean surface waves play an important role in air–sea interactions by influencing surface fluxes, upper-ocean mixing, and coastal dynamics (Cavaleri et al., 2012). Wave-induced effects on flux parameterisations can affect wind speeds and precipitation (Rutgersson et al., 2012; Wu et al., 2019). In the WMC, MJO-driven wind variability enhances wave activity and modulates air–sea exchanges (Hilmi et al., 2018). Wave-state-dependent fluxes have been shown to improve MJO representation by reducing biases in winds and latent heat fluxes (Ikuyajolu et al., 2024). Waves also influence upper-ocean mixing, circulation, and stratification (Babanin, 2006; Breivik et al., 2015), with demonstrated benefits for ocean and coastal forecasts (Bruciaferri et al., 2021; Wang et al., 2022; Jing et al., 2025). These findings highlight the importance of including wave processes in coupled systems.

Increasing horizontal resolution further improves convection representation, as finer grids allow explicit treatment of small-scale processes (Li et al., 2017). Convection-permitting resolutions (~1–3 km) substantially improve the simulation of the diurnal precipitation cycle over the Maritime Continent (Argüeso et al., 2020). Over the WMC, a 1.5 km configuration outperforms coarser (~4.5 km) models in representing rainfall (Heng et al., 2020). Coupled systems also benefit from higher resolution; for example, a 2.2 km atmosphere–ocean configuration improves diurnal variability and SST–precipitation

relationships compared to coarser (~12 km) models (Howard et al., 2024). Together, these results emphasise the need for high-resolution coupled modelling to reduce persistent biases in WMC simulations.

Despite these advances, significant challenges remain in representing air–sea interactions and associated precipitation processes over the WMC. Many existing studies either employ atmosphere-only convection-permitting models without interactive ocean feedbacks, or coupled systems at coarser resolutions that rely on parameterised convection. In addition, wave coupling is often neglected, further limiting the representation of air–sea momentum exchange and upper-ocean processes. Consequently, few studies have combined kilometre-scale, convection-permitting atmospheric models with fully coupled ocean–wave components in the WMC region.

Precipitation is a particularly relevant target for such a system. It is a key component of the WMC weather and climate system, characterised by a pronounced diurnal cycle, offshore propagation of convection, and strong sensitivity to air–sea interactions, and it has significant societal impacts, including flooding and landslides across the region. However, previous studies have reported mixed impacts of atmosphere–ocean coupling on precipitation, depending on model configuration and region (Aldrian et al., 2005; Wei et al., 2014; Xue et al., 2020), highlighting the need to assess these impacts in a kilometre-scale coupled system that resolves convection explicitly.

To address these gaps, we develop and evaluate a 1.5 km convection-permitting coupled atmosphere–ocean–wave modelling system for the WMC. The primary objective of this study is to document the development of cSINGV v1.0, a fully coupled system enabling two-way interactions between the atmosphere, ocean, and waves at kilometre scale, which represents the main technical contribution of this work, and to provide an initial assessment of its performance relative to the uncoupled atmospheric configuration, with a particular focus on the representation of precipitation, diurnal variability, and air–sea interactions. The study distinguishes three aspects: (i) the development and configuration of the individual regional ocean and wave components; (ii) the implementation of the coupled atmosphere–ocean–wave system; and (iii) an initial evaluation of the fully coupled configuration. The manuscript is not intended to present a comprehensive optimisation or sensitivity analysis of all coupling parameters and feedback processes.

The remainder of this paper is organised as follows. Section 2 describes the model components and the coupled modelling framework. Section 3 outlines the experimental design, datasets, and evaluation methodology. Section 4 presents the model evaluation results, including the assessment of coupling effects. Finally, Section 5 summarises the main findings and conclusions, while Section 6 outlines future developments.

2 Model components and coupled system design

2.1 Overview of the cSINGV system

The cSINGV modelling system is a high-resolution (1.5 km) regional coupled atmosphere–ocean–wave framework developed for the WMC. It integrates a convection-permitting atmospheric model based on the Met Office Unified Model (UM), an ocean model based on the Nucleus for European Modelling of the Ocean (NEMO), and a spectral wave model based on

WAVEWATCH III (WW3), within a unified coupling framework based on the UK Met Office Regional Coupled Suite (RCS) (Castillo et al., 2022).

In this study, the atmospheric component (hereafter referred to as cSINGV_A) is based on the numerical weather prediction system SINGV, used at the Meteorological Service Singapore (MSS). The ocean and wave components (hereafter referred to as cSINGV_O and cSINGV_W, respectively) have been newly developed and configured for the WMC. The model domain spans 94.6°E–109.36°E and 5.7°S–8.13°N (Fig. 1), covering the complex coastal and shelf regions of the WMC. The system is designed to capture multiscale interactions, including diurnal variability, coastal processes, and air–sea–wave coupling, which are critical for accurately representing weather and climate in this region. The individual component models and the coupling framework are described in detail in the following sections.

2.2 Atmospheric and land surface model (cSINGV_A)

The atmosphere and land surface components in cSINGV are based on a fixed-resolution latitude–longitude grid with a horizontal spacing of 1.5 km over the model domain. It is a fully non-hydrostatic model with a terrain-following vertical coordinate system, consisting of 80 vertical levels extending up to a model top of 38.5 km. The vertical resolution is approximately 5 m near the surface and 1.45 km at the model top, with a 60-second time step for model integration. The configuration is consistent with the MSS operational numerical weather prediction system, SINGV (Huang et al., 2019).

Land surface processes are represented using the Joint UK Land Environment Simulator (JULES v7.5; Best et al., 2011), which includes nine surface fraction types. The atmosphere and land surface components are compiled as a single executable and coupled implicitly at each model time step following Best et al. (2004), ensuring consistent land–atmosphere interactions. Physical parameterisations include the Prognostic Cloud fraction and Prognostic Condensate (PC2) scheme (Wilson et al., 2008), as used in previous implementations (Huang et al., 2019). The boundary-layer parameterization follows a blending approach developed by Boutle et al. (2014), which combines the one-dimensional scheme of Lock et al. (2000) with the three-dimensional Smagorinsky-Lilly scheme (Lilly, 1962). The cloud microphysics scheme is based on Wilson and Ballard (1999), while radiation processes are modelled using the Edwards and Slingo (1996) scheme, which includes six shortwave bands and nine longwave bands (Manners et al., 2012).

The configuration used in this study (cSINGV_A) adopts the Regional Atmosphere and Land v2 in the Tropics (RAL2-T) configuration (Bush et al., 2023). This configuration is used as the baseline atmospheric system onto which the ocean and wave components are coupled. SST is prescribed from OSTIA and updated daily in cSINGV_A to provide a consistent reference for comparison with the coupled simulations. Ocean surface currents are set to zero, and the Charnock parameter is prescribed as a constant value of 0.011 over all ocean points (Bush et al., 2023). No additional tuning or modifications are applied beyond this configuration.

2.3 Ocean model development and configuration (cSINGV_O)

The ocean component was newly configured and developed for application over the WMC. The ocean component, cSINGV_O, is based on version 4.0.4 of the NEMO (NEMO development team, 2021), configured at 1.5 km horizontal resolution. NEMO is a primitive-equation, hydrostatic model extensively used in climate and operational forecast applications (Madec et al., 2017). The model employs an orthogonal curvilinear coordinate system with Arakawa C-grid staggering for its horizontal grid, and the bathymetry is derived from the General Bathymetric Chart of the Oceans (GEBCO) dataset (https://www.gebco.net/data-products/historical-data-sets#gebco_2020, last access: 26 February 2026).

Featuring 51 vertical levels within a terrain-following coordinate system, the model incorporates the stretching function by Siddorn and Furner (2013). In our study, the ocean model configurations utilize baroclinic time steps set at 60 seconds. The Generic Length Scale (GLS) turbulence model (Umlauf and Burchard 2003) is employed to calculate turbulent viscosities and diffusivities. For the computation of the bottom drag coefficient, an implicit form of non-linear parameterization with a log-layer formulation is applied, setting the minimum and maximum drag coefficients at 0.0001 and 0.15, respectively. The Flather boundary condition (Flather 1987) is adopted for SSH and barotropic velocities, while a flow relaxation scheme (FRS, Davies 1976) is implemented for tracers and baroclinic velocities at the lateral open ocean boundaries.

The configuration (cSINGV_O) is largely based on the regional NEMO setup of Thompson et al. (2021), with additional modifications introduced during the upgrade from version 3.6 to 4.0.4 (Table S1). Prior to coupling, standalone ocean-only sensitivity experiments were conducted to establish a stable and physically credible regional NEMO baseline. These experiments tested configuration choices, including the light-penetration scheme, and the selected configuration improved the representation of SST in both deep-ocean and shallow-shelf regions. The experiments were intended solely to establish suitable behaviour of the standalone ocean component, and the selected configuration was subsequently held fixed in the coupled simulation.

2.4 Wave model development and configuration (cSINGV_W)

The wave component, cSINGV_W, was newly configured and tuned for the WMC. It is based on version 7.12 of the third-generation spectral wave model WW3 (Tolman, 2014), developed by the U.S. National Centers for Environmental Prediction. To better represent the complex coastlines around Singapore, the model is configured with a two-tier spherical multiple-cell (SMC) grid (Li, 2012), using the same computational domain and bathymetry as the ocean component. The SMC approach enables multi-resolution meshes, allowing fine-scale representation of coastlines and small islands while maintaining coarser resolution in the open ocean. This feature provides more effective refinement of coastal areas compared to a regular WW3 grid (Li et al., 2019), which is particularly beneficial in the coastal environment of the WMC. The model grid has a resolution of approximately 1.5 km in coastal regions, expanding to 3 km in offshore areas.

The model employs the ST4 source term package (Ardhuin et al., 2010) to represent wave growth and dissipation processes. Nonlinear wave–wave interactions are parameterised using the discrete interaction approximation (NL1; Hasselmann et al.,

1985), while shallow-water processes include depth-induced breaking (DB1; Battjes and Janssen, 1978) and bottom friction (BT1; Hasselmann et al., 1973). Wave propagation is computed using a second-order upstream non-oscillatory scheme (UNO; Li, 2008), and dispersion correction is applied through the PR2 option to mitigate the garden sprinkler effect (Booij and Holthuijsen, 1987). Wind input and stress calculations are handled internally within the source term formulation (FLX0), with additional options for wind and current interpolation (WNT1, WNX1, CRT1, CRX1). In the coupled configuration, the spatial remapping of the atmospheric wind and ocean-current fields between the component grids is performed by OASIS3-MCT using precomputed remapping weights, and each component evolves with its own time step between coupling exchanges and therefore compiled with WNT0 and CRT0. A summary of the model configuration and compilation switches is provided in Table S2.

Specific adjustments to key parameters, including the wave growth parameter *betamax* and shallow-water physics options, were made for application to the WMC. These parameters were selected during the standalone development of the regional WW3 configuration, which was forced by winds from cSINGV_A, before the fully coupled experiments were conducted. They were subsequently held fixed in the coupled simulation and were not adjusted to improve the performance of the coupled model. The tuning strategy and sensitivity experiments are described in Appendix A.

2.5 Coupled modelling framework

The coupled modelling system is implemented using RCS, which provides a flexible framework for integrating multiple model components using the cylc workflow engine (Oliver et al., 2019). Coupling between the atmosphere, ocean, and wave components is achieved through the OASIS3-MCT coupler (Craig et al., 2017), enabling the exchange of fluxes and state variables between components.

The configuration used in this study is based on the RCS suite (suite ID: u-bf945), with a dedicated *cSINGV* branch developed for this application and available via the Met Office repository (https://code.metoffice.gov.uk/svn/roses-u/b/f/9/4/5/u-bf945_add_cSINGV_br). This branch provides the specific coupling setup and workflow required for the coupled system, ensuring reproducibility of the model configuration.

The atmosphere, ocean, and wave components operate on their native grids and exchange variables at an hourly coupling frequency. The one-hour coupling interval was selected as a practical compromise between computational cost, coupling overhead, and the need to represent evolving regional air–sea interactions. Previous work over the Maritime Continent found that hourly or more frequent coupling better represented SST variability and convection (Zhao and Nasuno, 2020). However, the hourly interval is a design choice rather than a demonstrated optimum. Shorter intervals may better represent rapidly evolving convection and high-frequency air–sea interactions (Makrygianni et al., 2026).

The framework supports two-way interactions between components, allowing for feedbacks such as the influence of SST on atmospheric fluxes, wave-dependent surface roughness effects, and the impact of ocean currents on wave evolution. A schematic overview of the coupling architecture is shown in Fig. 2, and the exchanged variables are listed in Table 1. In the

fully coupled atmosphere–ocean–wave configuration (cSINGV), the atmosphere supplies the 10 m zonal and meridional wind components to WW3, and WW3 provides NEMO with the zonal and meridional components of the stress transmitted to the ocean after accounting for the evolving wave field. This coupling strategy is consistent with established atmosphere–wave–ocean coupling frameworks (e.g., Breivik et al., 2015, their Fig. 8).

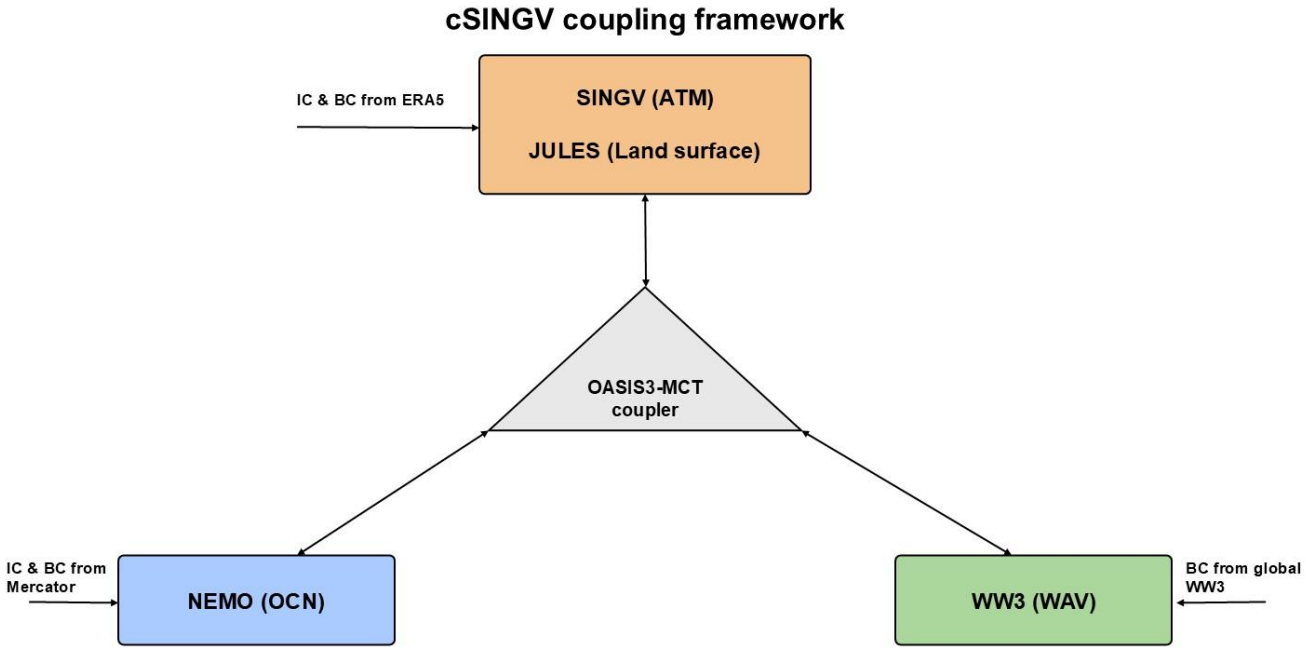


Figure 2: Schematic representation of the cSINGV coupled atmosphere–ocean–wave modelling system. The atmospheric model (SINGV; Unified Model–based configuration) is coupled with the Joint UK Land Environment Simulator (JULES) for land surface processes, the Nucleus for European Modelling of the Ocean (NEMO) for ocean dynamics, and the WAVEWATCH III (WW3) for wave processes. Coupling between components is achieved through the OASIS3-MCT coupler, which exchanges fluxes and state variables between the atmosphere (A), ocean (O), and wave (W) components at hourly intervals. IC and BC denote initial conditions and lateral boundary conditions, respectively.

Table 1: Variables exchanged through OASIS3-MCT between the component models of cSINGV.

From → To	Exchanged variables
Atmosphere → Ocean	Non-solar net surface heat flux
	Solar surface heat flux
	Rainfall rate
	Snowfall rate
	Freshwater evaporation rate
	Mean sea-level pressure

Ocean → Atmosphere	Sea surface temperature Zonal and meridional surface currents
Atmosphere → Wave	10 m zonal and meridional wind components
Wave → Atmosphere	Charnock parameter
Ocean → Wave	Zonal and meridional surface currents
Wave → Ocean	Significant wave height Zonal and meridional surface Stokes drift velocities Mean wave period Zonal and meridional components of the surface atmospheric stress transmitted to the ocean.

3 Experimental design, datasets, and evaluation methodology

3.1 Experimental design

Simulations are conducted for January–June 2019 using both standalone and coupled configurations:

- Atmospheric-only (cSINGV_A)
- Ocean-only (cSINGV_O)
- Wave-only (cSINGV_W)
- Fully coupled system (cSINGV)

Atmospheric lateral boundary conditions are provided by reanalysis data, while ocean initial and boundary conditions are obtained from ocean reanalysis products. Wave boundary conditions are derived from a high-resolution global WW3 simulation using an SMC grid.

3.2 Datasets

The atmospheric model lateral boundary conditions are provided by the 3-hourly European Centre for Medium-Range Weather Forecasts (ECMWF) reanalysis, ERA5 (Hersbach et al., 2020). Ocean model initial and lateral boundary conditions are obtained from the daily Mercator Ocean reanalysis (Lellouche et al., 2021). Wave boundary conditions are derived from a high-resolution global WW3 simulation using a four-tier spherical multiple-cell (SMC61250) grid, with resolutions of 50, 25, 12, and 6 km from the open ocean to coastal regions (Li, 2019; Kumar et al., 2025), forced by ERA5 winds. Tidal forcing at the ocean lateral boundaries is prescribed using tidal elevations and currents from the Finite Element Solution dataset (FES2014b; Lyard et al., 2021; https://www.aviso.altimetry.fr/en/data/products/auxiliary-products/global-tide-fes.html). River runoff is represented using monthly climatological fields from Dai and Trenberth (2002). In addition, monthly chlorophyll concentrations from the Sea-viewing Wide Field-of-view Sensor (SeaWiFS; Hooker and McClain, 2000) are used in the ocean model to parameterise light absorption and its influence on the upper-ocean heat budget.

For model evaluation, multiple observational and reanalysis datasets are used. Precipitation is evaluated against the Integrated Multi-satellite Retrievals for Global Precipitation Measurement (GPM IMERG V06B; Huffman et al., 2019: doi.org/10.5067/GPM/IMERG/3B-HH/06), hereafter referred to as GPM, which provides reliable estimates over Southeast Asia (e.g. Da Silva et al., 2021). Three-hourly 10 m wind speed and 2 m air temperature observations are obtained from the World Meteorological Organization (WMO) MetDB database (Met Office, 2008). SST is evaluated using the Operational Sea Surface Temperature and Sea Ice Analysis (OSTIA: https://doi.org/10.48670/moi-00168) dataset and the GLORYS12V1 product from the Copernicus Marine Environment Monitoring Service (CMEMS; Lellouche et al., 2021: https://doi.org/10.48670/moi-00021). H_s is validated using multi-mission satellite altimeter observations (Piollé et al., 2022) obtained from CMEMS.

3.3 Evaluation methodology

Model performance is evaluated using a range of statistical metrics. The root mean square error (RMSE) is used to assess 10 m wind speed, 2 m air temperature, SST, and H_s, and is defined as:

$$\mathrm{RMSE} = \sqrt{\frac{1}{N}\sum_{i=1}^{N}(M_i - O_i)^2}$$

where M_i and O_i denote the modelled and observed values, respectively, and N is the number of samples.

For wave evaluation, additional metrics are applied. The bias is defined as:

$$\mathrm{Bias} = \frac{1}{N}\sum_{i=1}^{N}(M_i - O_i)$$

The Pearson correlation coefficient (r) is given by:

$$r = \frac{\sum_{i=1}^{N}(M_i - \bar{M})(O_i - \bar{O})}{\sqrt{\sum_{i=1}^{N}(M_i - \bar{M})^2}\sqrt{\sum_{i=1}^{N}(O_i - \bar{O})^2}}$$

The scatter index (SI), representing the normalised RMSE, is defined as:

$$\mathrm{SI} = \frac{\mathrm{RMSE}}{\bar{O}}$$

Distributional agreement between modelled and observed H_s is assessed using the Kolmogorov–Smirnov (KS) statistic (Massey, 1951), defined as:

$$\mathrm{KS} = \max \mid F_m(x) - F_o(x) \mid$$

where $F_m(x)$ and $F_o(x)$ are the cumulative distribution functions of modelled and observed values, respectively.

Probability distribution functions (PDFs) were estimated using kernel density estimation (KDE; Parzen, 1962), implemented via KDEpy (Odland, 2018). For precipitation, the Fraction Skill Score (FSS; Roberts and Lean, 2008) is used to evaluate the spatial representation of rainfall. It is computed for selected precipitation thresholds and neighbourhood sizes and is defined as:

$$\mathrm{FSS} = 1 - \frac{\sum(P_f - P_o)^2}{\sum(P_f^2 + P_o^2)}$$

where P_f and P_o represent the fractional coverage of forecast and observed precipitation exceeding a specified threshold within a given neighbourhood. FSS is computed within the evaluation domain indicated by the red box in Fig. 1.

To assess whether differences between cSINGV and cSINGV_A are distinguishable from day-to-day variability, paired analyses were applied to the daily scores of the two configurations. For FSS, the mean paired difference (ΔFSS = cSINGV − cSINGV_A) and its 95 % confidence interval were calculated from the paired daily differences. For the RMSE of 10 m wind speed and 2 m air temperature, the daily paired differences ($\Delta\mathrm{RMSE} = \mathrm{RMSE}_{\mathrm{cSINGV_A}} - \mathrm{RMSE}_{\mathrm{cSINGV}}$) were examined using a sign test. Daily precipitation bias relative to GPM was also calculated for both configurations.

The evaluation of atmospheric variables was performed using the MetPlus framework, which provides a standardized environment for model verification and ensures reproducibility of the analysis (https://metplus.readthedocs.io/en/latest/).

4 Model evaluation and coupling impacts

This section presents the evaluation of the cSINGV system with a focus on the newly developed ocean and wave components, followed by an assessment of the impact of atmosphere–ocean–wave coupling. The atmospheric component used in this study corresponds to the SINGV configuration, which has been extensively evaluated in previous studies. Therefore, only its role as a reference configuration is considered here.

We first evaluate the standalone ocean (cSINGV_O) and wave (cSINGV_W) components to establish their ability to represent key marine processes in the WMC. These component-level assessments are included as baseline checks: they establish whether the ocean and wave components reproduce the observed SST and H_s adequately before their fields are used interactively in the coupled system. Without such an assessment, biases originating in an individual component could be incorrectly interpreted as coupling errors or as evidence of coupling benefits. We then assess the fully coupled system (cSINGV) relative to the uncoupled atmospheric configuration (cSINGV_A) to examine the influence of coupling, and assess whether the fidelity of the ocean and wave components is maintained in the coupled configuration.

4.1 Ocean model evaluation (cSINGV_O)

The ocean component is evaluated through comparisons of SST with OSTIA and CMEMS reanalysis datasets for the period January–June 2019. Given that SST is the key variable linking the ocean to the atmosphere in the coupled system, the evaluation focuses on its representation.

The WMC region is characterised by two distinct ocean regimes: the shallow Sunda Shelf in the South China Sea (SCS) and the deeper Indian Ocean basin west of Sumatra (Fig. 1). To assess model performance across these contrasting environments, the analysis is conducted separately for these regions (Fig. S1). Figure 3 shows the time series of domain-averaged RMSE of daily SST relative to OSTIA for (i) the full domain, (ii) the Indian Ocean, and (iii) the South China Sea over the six-month simulation period.

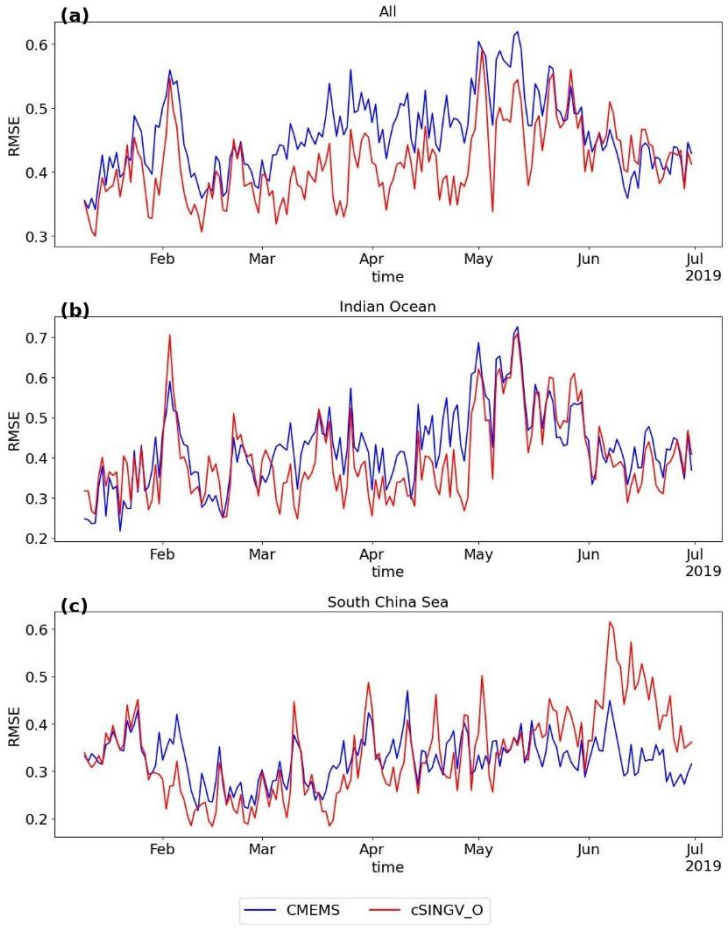


Figure 3: Time series of daily domain-averaged RMSE of SST relative to OSTIA for the cSINGV_O simulation (red) and CMEMS reanalysis (blue) for January–June 2019, shown for (a) the full domain, (b) the Indian Ocean region, and (c) the South China Sea (Sunda Shelf).

The model reproduces SST variability well across both regions, with domain-averaged RMSE values generally below 0.5 °C throughout the simulation period. Some deviations are evident in the Indian Ocean during February and May, but the model captures the overall temporal variability and maintains errors comparable to CMEMS. In the SCS, SST variability is also well

represented, with consistent agreement across the simulation period. Additional comparison with the regional NEMO configuration of Thompson et al. (2021) shows that the large-scale SST patterns are well reproduced (Fig. S2), and domain-averaged RMSE values are comparable (Fig. S3), providing further confidence in the ocean configuration.

4.2 Wave model evaluation (cSINGV_W)

Following the model tuning described in Appendix A, the cSINGV_W configuration is evaluated against multi-mission satellite altimeter observations for January 2019 over the full domain and two subregions: the Indian Ocean and the South China Sea, representing distinct wave regimes. January 2019 was selected as it includes Tropical Storm Pabuk, providing a strong-wind case suitable for assessing wave growth.

The model reproduces the variability of H_s well across the domain (Fig. 4). Scatter comparisons show strong agreement with observations, with most values distributed close to the 1:1 line. For the full domain, the RMSE is approximately 0.2 m, with a correlation coefficient exceeding 0.926. Performance is slightly reduced in the Indian Ocean (RMSE = 0.21 m), possibly reflecting the greater influence of remotely generated swell, while improved agreement is observed in the South China Sea (RMSE = 0.185 m), where locally generated wind sea is expected to be more important.

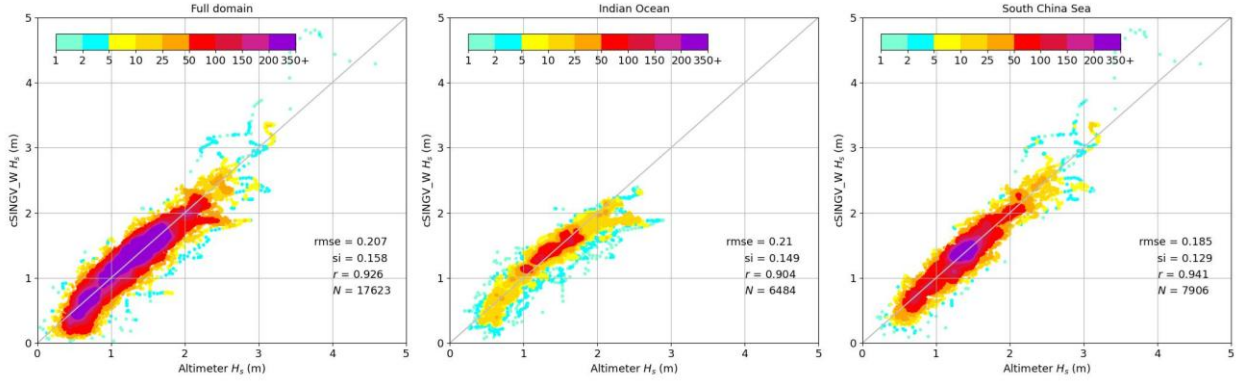


Figure 4: Validation of stand-alone cSINGV_W model against altimeter significant wave height (H_s) for January 2019 for the (a) whole domain, (b) Indian Ocean and (c) South China Sea region.

To assess the performance of the selected configuration (*betamax* = 1.75) beyond the January strong-wind case, the cSINGV_W evaluation was extended to January–June 2019 (Fig. S4 and Table S3). Across the six months, RMSE ranges from 0.179 to 0.287 m, the correlation coefficient from 0.910 to 0.966, and SI from 0.150 to 0.270, with a negative monthly bias ranging from −0.018 to −0.195 m. Performance is strongest in January–February and weaker in April–May, but correlations remain above 0.91 in every month. These results support the suitability of *betamax* = 1.75 for the standalone regional wave configuration over the evaluation period.

Overall, the standalone ocean and wave evaluations demonstrate that the individual components provide a credible representation of key marine processes, forming a strong foundation for the development of the fully coupled cSINGV system.

4.3 Evaluation of the coupled system (cSINGV)

Building on the evaluation of the standalone ocean and wave components, we now examine the performance of the fully coupled system (cSINGV) by comparing it with the atmosphere-only configuration (cSINGV_A). It should be noted that cSINGV_A uses prescribed OSTIA SST, whereas cSINGV uses dynamically evolving SST from the ocean model. Therefore, the comparison does not represent a fully controlled coupling experiment, but rather provides insight into the combined effects of the interactive coupling processes represented in the coupled configuration.

Two further differences between the configurations should be considered. First, SST in cSINGV_A is updated daily and remains fixed within each day, whereas cSINGV produces appreciable and spatially heterogeneous sub-daily SST variability. The mean daily SST range in cSINGV—calculated as the difference between the maximum and minimum of the 24 hourly values and then averaged over January–June 2019—is typically 0.5–0.75 °C over the open ocean and exceeds 1 °C in some shallow and coastal waters, including the Malacca Strait and waters surrounding Sumatra (Fig. S5). This variability may modify near-surface air–sea temperature and humidity gradients, thereby influencing the timing and magnitude of turbulent heat fluxes and convection on diurnal timescales. Consequently, differences between the two configurations, particularly at diurnal timescales, cannot be attributed solely to two-way coupling, as they may also reflect the presence of sub-daily SST variability in cSINGV. Second, cSINGV_A uses a fixed Charnock parameter of 0.011, whereas cSINGV uses a WW3-supplied Charnock parameter that varies with the evolving sea state, exhibiting spatial and month-to-month variability (not shown). The configurations therefore differ in their representation of aerodynamic roughness, which may contribute to the simulated differences in surface winds and turbulent fluxes. Accordingly, (cSINGV_A) serves as a reference against which the combined response to interactive SST, wave-dependent roughness, and other coupling pathways in cSINGV is assessed.

4.3.1 Precipitation

We first assess precipitation, examining how the coupled (cSINGV) and uncoupled (cSINGV_A) configurations represent key rainfall characteristics.

To provide a qualitative overview, Hovmöller diagrams of daily accumulated precipitation were constructed using GPM satellite observations, together with cSINGV and cSINGV_A simulations, across longitudes 95.5°E–108°E for January–June 2019 (Fig. 5). Both model configurations reproduce the broad temporal and spatial variability of rainfall seen in GPM, although they tend to produce more moderate and intense rainfall compared to the observations. This representation is intended to illustrate the large-scale temporal and longitudinal evolution of precipitation and to examine whether coupling produces a systematic shift in its distribution, rather than to quantify model skill. To quantify the differences, the daily precipitation bias relative to GPM was calculated for both configurations (Fig. S6). Both simulations exhibit an overall wet bias, but its domain- and period-mean magnitude is larger in cSINGV (+0.96 mm day^{-1}) than in cSINGV_A (+0.55 mm day^{-1}). Coupling therefore exacerbates the mean wet bias by approximately 0.41 mm day^{-1} during the evaluation period, although the impact varies substantially with longitude and time and includes periods and locations in which the bias is reduced. The large-scale evolution

of rainfall is otherwise similar in the two configurations, indicating that coupling does not introduce spurious large-scale rainfall features.

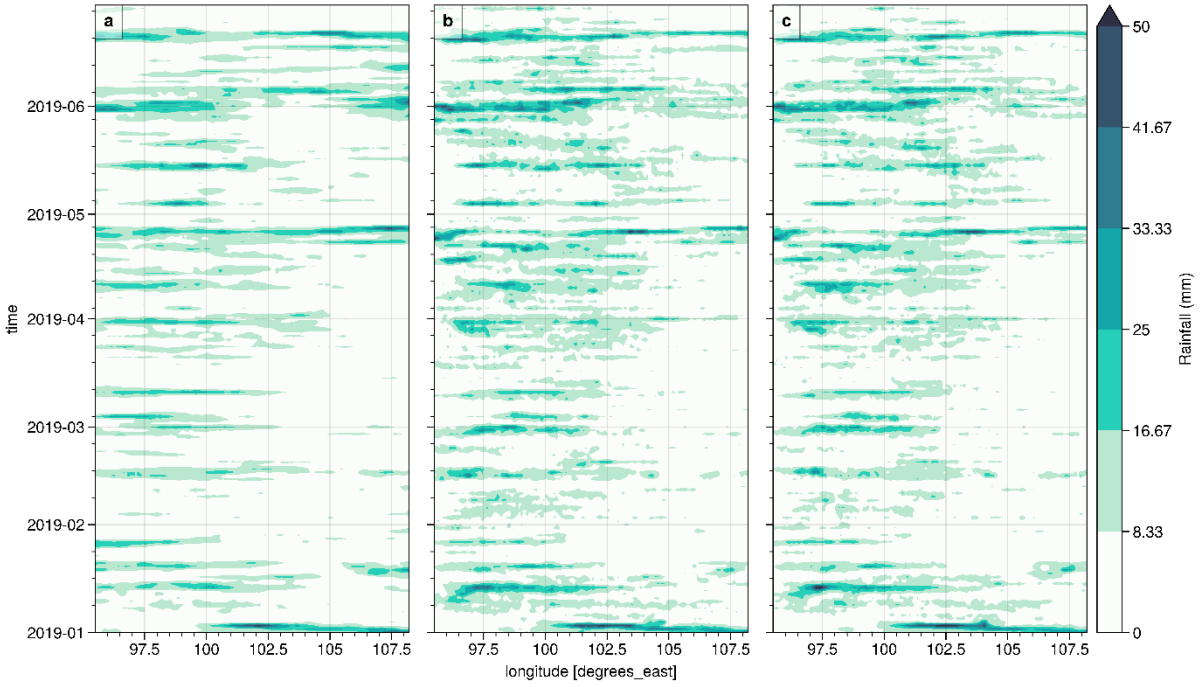


Figure 5: Hovmöller diagrams of daily rainfall (mm/day) averaged over latitude from January to June 2019 for (a) GPM observations, (b) the coupled model simulation (cSINGV), and (c) the uncoupled simulation (cSINGV_A).

To quantify spatial performance, we evaluate the FSS, which measures the agreement between simulated and observed rainfall patterns, with GPM serving as the reference dataset. FSS is particularly well-suited for evaluating precipitation, as it is less sensitive to exact grid-point matches compared to traditional metrics. Figure 6 presents FSS as a function of neighbourhood width for March and June 2019, selected as representative months. Two precipitation thresholds are considered: ≥0.1 mm and ≥10 mm. For March, across a range of neighbourhood sizes and precipitation thresholds, the coupled configuration generally exhibits higher FSS values than the uncoupled configuration, indicating improved spatial organisation of precipitation. At higher thresholds, both configurations exhibit lower skill, although cSINGV maintains a modest advantage. Similar behaviour is observed in June and across the remaining months, although differences are generally smaller for other months (January, February, April, and May; Fig. S7). To assess whether these differences are distinguishable from day-to-day variability, the mean paired difference in daily FSS (ΔFSS = cSINGV − cSINGV_A) was calculated for January–June 2019 (Fig. S8). For rainfall ≥0.1 mm day^{-1}, cSINGV shows a consistent improvement of approximately 0.020–0.026 across all neighbourhood widths, with the 95 % confidence interval remaining above zero. For rainfall ≥10 mm day^{-1}, the improvement is smaller

(approximately 0.002–0.007) and is only marginally significant at the largest neighbourhood widths. Thus, the coupled improvement is robust for overall rainfall occurrence but less conclusive for heavier rainfall.

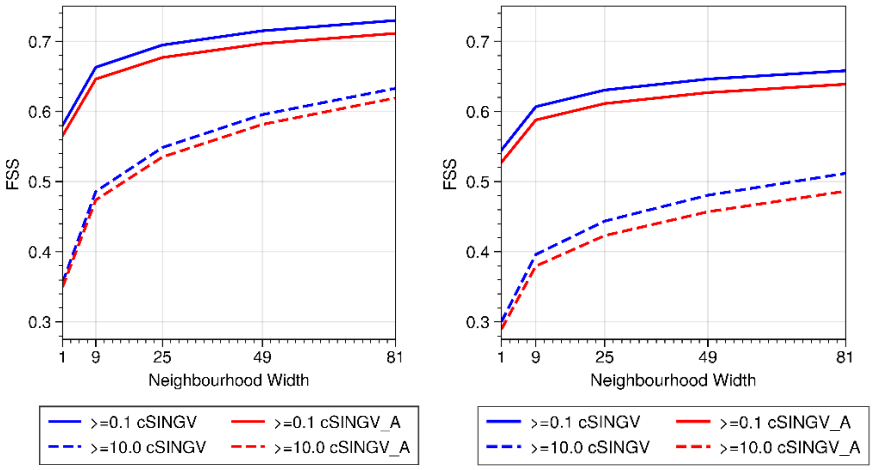


Figure 6: FSS as a function of neighbourhood width for March (left) and June (right) 2019, computed within the evaluation domain (red box in Fig. 1) and evaluated at two precipitation thresholds: ≥0.1 mm (solid lines) and ≥10.0 mm (dashed lines). Blue lines represent the coupled model (cSINGV) simulations, while red lines represent the uncoupled model (cSINGV_A) simulations. The neighbourhood width is expressed in terms of grid cells; for example, a width of 81 corresponds to a 9 × 9 grid box, equivalent to approximately 13.5 km × 13.5 km at the model resolution of 1.5 km.

We next examine the diurnal cycle of precipitation, a defining feature of rainfall over the WMC linked closely to land–sea breezes, convection, and ocean–atmosphere interactions. Evaluating the model's ability to reproduce these cycles therefore provides an important test of its representation of regional processes. Figure 7 shows the mean diurnal cycle averaged over January–June 2019 for land and sea regions. Over land, both cSINGV and cSINGV_A reproduce the general shape of the diurnal cycle but exhibit a phase lead of approximately 2–3 hours relative to GPM observations, along with an overestimation of peak intensity. Differences between the two configurations are small, indicating limited impact of coupling over land. In contrast, over the ocean, the cSINGV configuration more closely reproduces the observed timing and amplitude of nocturnal rainfall, while the cSINGV_A simulation underestimates rainfall and deviates more from observations. This indicates that coupling improves the representation of oceanic convection, which is closely linked to SST variability and surface flux feedbacks. Although both configurations underestimate precipitation overall, cSINGV shows improved agreement with the observed cycle across most hours. The overestimation of the precipitation peak over land, together with the underestimation over the ocean, is consistent with the land-wet/ocean-dry bias reported in long-term 2 km SINGV-RCM simulations over the WMC region (Prasanna et al., 2025, their Fig. 7).

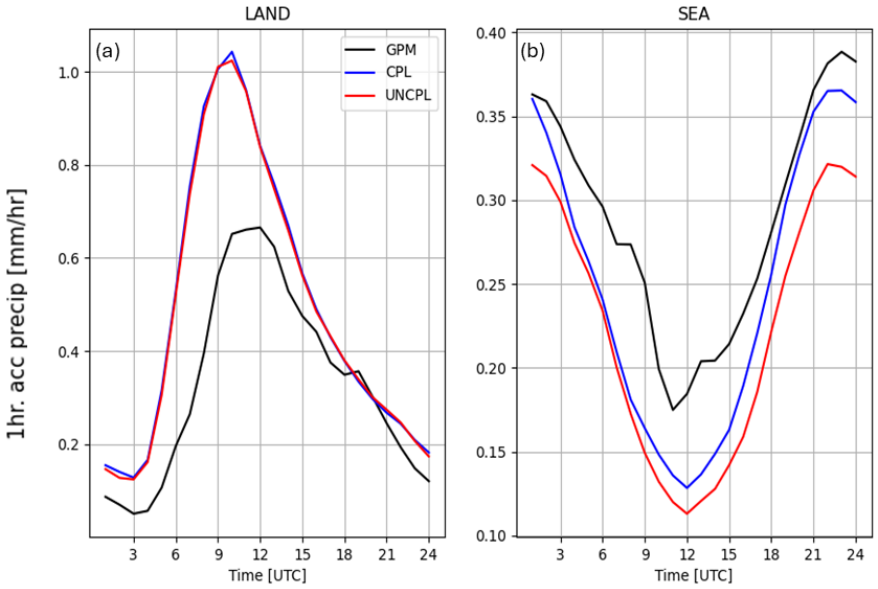


Figure 7: Mean diurnal cycle of precipitation (mm h^{-1}) over (a) land and (b) sea for January–June 2019 from GPM (black), the coupled simulation cSINGV (blue), and the uncoupled simulation cSINGV_A (red). Time is in UTC.

Another key feature of the WMC precipitation system is the offshore propagation of convection. Convection typically initiates over land during the afternoon, peaks in the evening, and subsequently propagates offshore during the night and early morning hours (Peatman et al., 2025). This behaviour strongly influences coastal rainfall and provides a useful benchmark for model evaluation. Figure 8 shows the diurnal evolution of precipitation along a coastal transect across western Sumatra (location shown in Fig. S9) for June 2019. The x-axis represents distance relative to the coastline (negative values indicating the offshore direction), while the y-axis denotes local time (LT).

In GPM observations, rainfall develops over land in the afternoon and propagates offshore during the evening or night with maxima extending progressively away from the coastline. The cSINGV configuration captures the observed propagation of rainfall from Sumatra toward the adjacent ocean more coherently than the cSINGV_A simulation. While some biases in intensity remain, the cSINGV better represents both the timing and spatial extent of offshore propagation, whereas the cSINGV_A configuration exhibits weaker and less organised structures. These differences suggest that coupling improves the representation of coastal rainfall variability.

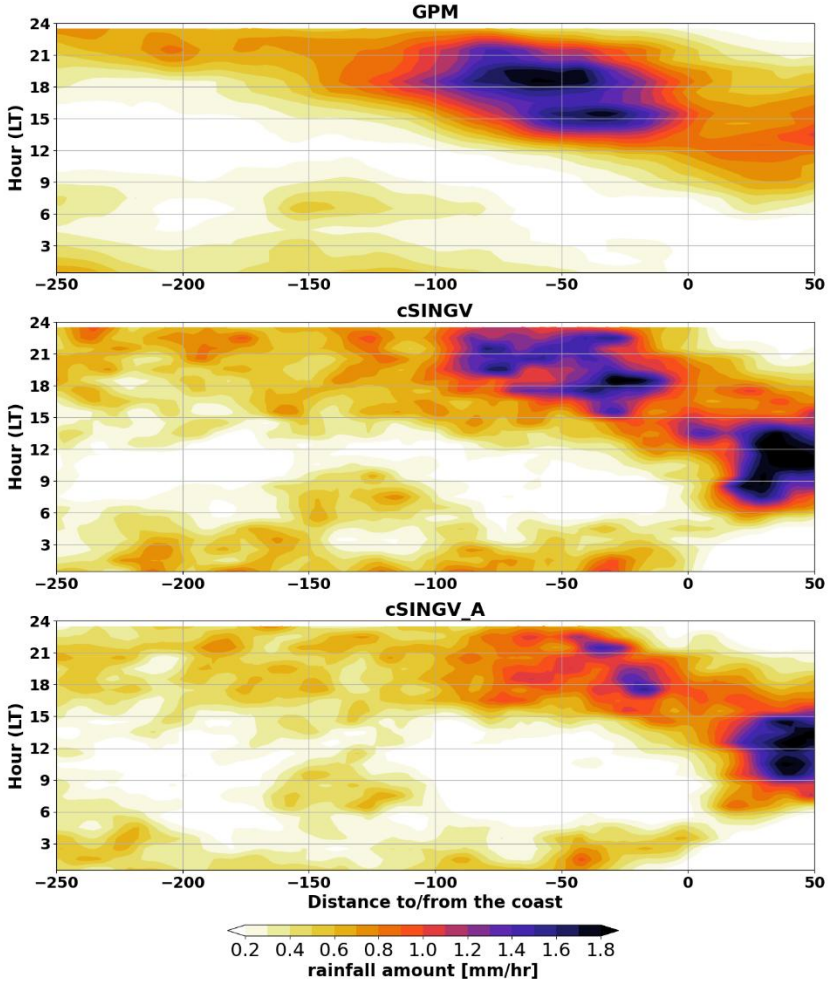


Figure 8: Diurnal rainfall Hovmöller diagram across the Sumatra transect for June 2019 derived from GPM observations (top), coupled simulation (cSINGV; middle), and uncoupled simulation (cSINGV_A; bottom). The y-axis shows local time (LT), and the x-axis represents distance relative to the western Sumatra coastline, with negative values indicating offshore (Indian Ocean) and positive values indicating inland regions. Shading denotes rainfall intensity (mm hr^{-1}).

Overall, the coupled configuration shows improved performance in representing key characteristics of precipitation over the WMC, including spatial organisation, the diurnal cycle over the sea, and offshore propagation, while differences over land remain limited.

4.3.2 Near-surface atmospheric variables

We next assess near-surface atmospheric variables using observations from WMO MetDB stations (Fig. S10). For 10 m wind speed (Fig. 9), both configurations show similar performance, with comparable agreement against observations and only minor differences between the coupled and uncoupled simulations. Similarly, 2 m air temperature (Fig. 10) is well represented in

both configurations, with small biases and limited sensitivity to coupling. These results suggest that near-surface atmospheric variables are less strongly influenced by coupling at the timescales considered in this study. Paired daily differences in RMSE confirm that the differences are not systematic (Figs. S11 and S12). The period-mean RMSE of 10 m wind speed is 1.96 m s^{-1} in cSINGV and 1.95 m s^{-1} in cSINGV_A, and that of 2 m air temperature is 1.82 K and 1.81 K, respectively. The daily differences change sign frequently, with slightly more days on which cSINGV_A has the lower RMSE, indicating that coupling provides no detectable improvement in these variables.

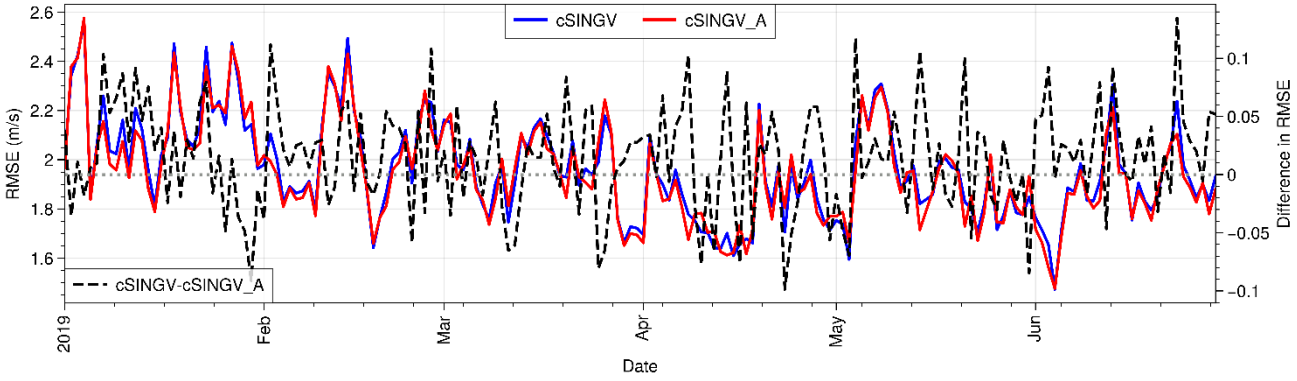


Figure 9: Daily mean wind speed rmse (m/s) for January-June 2019 against in-situ observations, for the coupled model (blue), uncoupled model (red), and the difference in rmse between the coupled and uncoupled model (black).

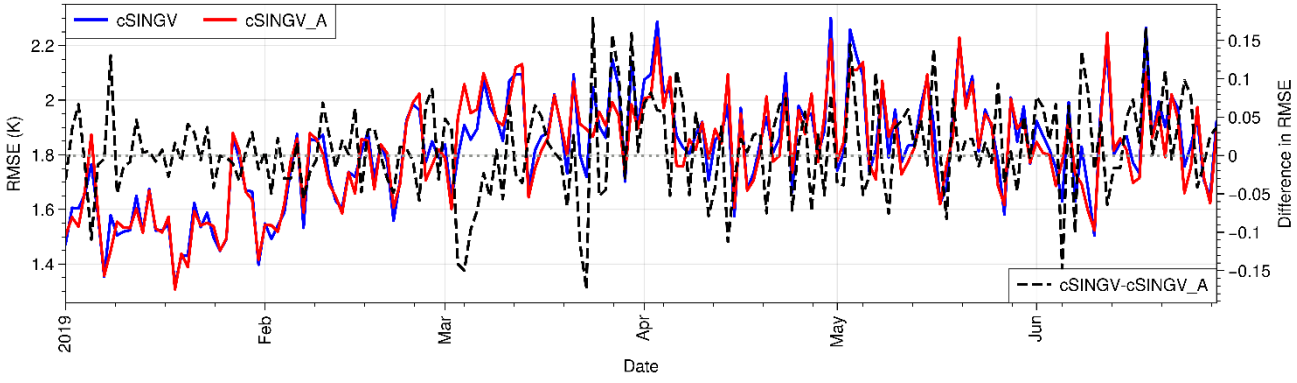


Figure 10: Daily mean 2 m air temperature rmse (K) for January-June 2019 against in-situ observations, for the coupled model (blue), uncoupled model (red), and the difference in rmse between the coupled and uncoupled model (black).

4.3.3 Sea surface temperature and significant wave height in the coupled system

To assess whether the fidelity of the ocean and wave components is maintained in the fully coupled system, SST and H_s from cSINGV were evaluated against observations. Figure 11 shows the daily spatially averaged SST from OSTIA, cSINGV, and

CMEMS, together with the daily spatial RMSE of cSINGV and CMEMS relative to OSTIA. cSINGV reproduces the seasonal evolution of the domain-mean SST, which warms from approximately 28.5–29 °C in January to about 30.5 °C in May, but exhibits a small warm bias relative to OSTIA that is largest in early May and from late May to June. The mean daily RMSE of cSINGV (0.45 °C) is comparable to, and slightly lower than, that of CMEMS (0.48 °C), although the cSINGV RMSE peaks at approximately 0.75 °C in early May. Monthly mean SST bias maps (Fig. S13) show that the warm bias is concentrated mainly along the coasts of Sumatra and the Malacca Strait, with monthly RMSE values between 0.25 and 0.39 °C.

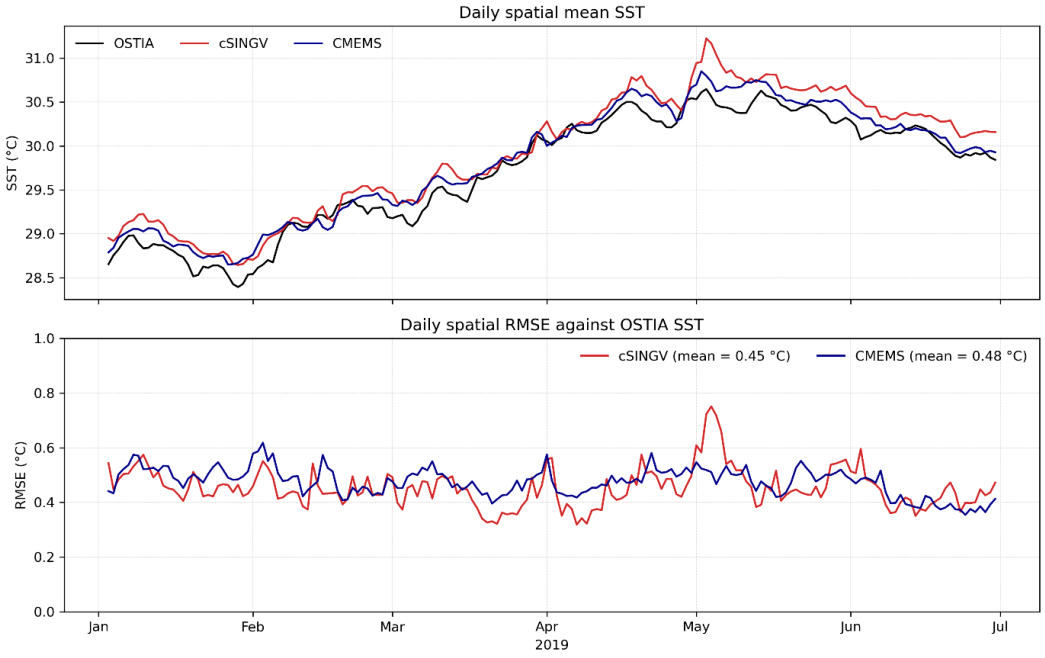


Figure 11: Daily spatially averaged sea surface temperature (SST) from OSTIA (black), the fully coupled cSINGV simulation (red), and CMEMS (blue) (top), and the corresponding daily spatial RMSE of cSINGV and CMEMS relative to OSTIA (bottom) over the model domain during January–June 2019.

Figure 12 shows the monthly comparison of H_s from cSINGV against satellite-altimeter observations (statistics in Table S4). The statistics are very close to those of the standalone cSINGV_W simulation (Table S3): RMSE ranges from 0.175 to 0.283 m, the correlation coefficient from 0.913 to 0.969, and SI from 0.152 to 0.267, with a negative bias between −0.025 and −0.194 m. Relative to cSINGV_W, the coupled simulation has slightly higher correlations in all months and slightly lower RMSE from February to May, but a slightly more negative bias in January–March and June.

Overall, these results show that the fidelity of the ocean and wave components is broadly maintained relative to their standalone configurations.

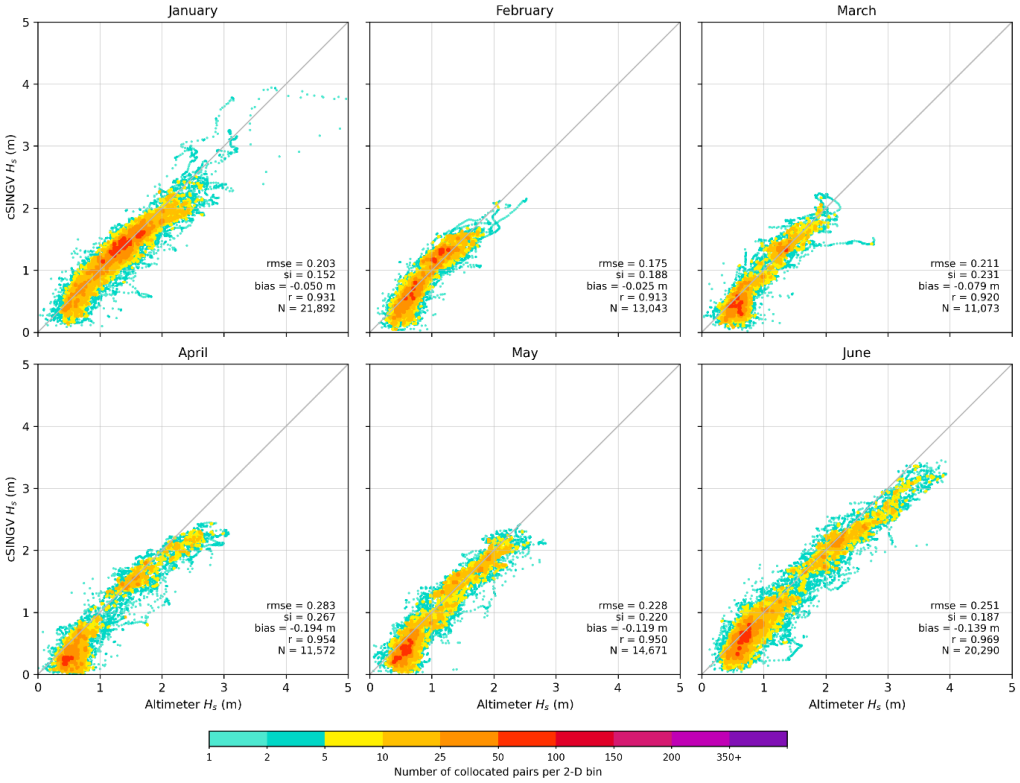


Figure 12: Monthly comparison of significant wave height (H_S) from the fully coupled cSINGV simulation against satellite-altimeter observations over the full model domain during January–June 2019. Shading denotes the number of collocated pairs per bin; RMSE, scatter index (SI), bias, correlation coefficient (r), and number of collocations (N) are given in each panel.

4.4 Impact of atmosphere–ocean–wave coupling (cSINGV vs cSINGV_A)

To further assess the impact of coupling at the event scale, we examine a set of Sumatra squall events. Sumatra squall lines are among the most frequent and impactful convective systems over the WMC, often producing intense rainfall, strong winds, and localized flooding (Lo and Orton, 2016). These systems typically initiate along the western coast of Sumatra and propagate eastward across the Straits of Malacca toward Peninsular Malaysia and Singapore. Their evolution is influenced by both land-based processes, such as orographic lifting and diurnal heating, and air–sea interactions, making them a useful benchmark for assessing the role of coupling in regional simulations.

In this section, we analyse a set of Sumatra squall events identified from the MSS squall database based on a threshold of maximum 1 h accumulated precipitation exceeding 50 mm. Five observed squall events satisfying this criterion occurred within the study domain during January–June 2019 (4 April, 27 April, 8 May, 19 May, and 3 June). Of these, only the 4 April and 27 April events were reproduced sufficiently well by at least one configuration to permit a process-based comparison; neither simulation reproduced the remaining three events, which were therefore not analysed further. Two additional events (3–4

September 2019 and 2–4 November 2020) were examined using separate simulations outside the continuous January–June 2019 experiment. The analysis is based on rotated Hovmöller diagrams constructed along a transect aligned with the typical propagation pathway from Sumatra to Singapore (Fig. 1), allowing a consistent assessment of the spatiotemporal evolution of convection.

4.4.1 Sumatra squall event: 25–27 April 2019

In late April 2019, two successive squall events developed under similar large-scale conditions (Fig. 13). The first system formed on 26 April along the western coast of Sumatra and propagated eastward across the Straits of Malacca, bringing heavy rainfall to Singapore. MSS reported 118.7 mm at Changi Airport, the highest daily total for April 2019 (maximum 1 h accumulation of 83.4 mm). A second squall formed on 27 April and affected parts of southern Sumatra and adjacent regions, where rainfall exceeding 200 mm triggered flooding and landslides (Paski et al., 2021).

We focus on the event impacting Singapore in the early hours of 27 April. GPM observations show a coherent convective system forming over Sumatra, propagating eastward, and reaching Singapore at approximately 00 UTC. The coupled simulation (cSINGV) captures this eastward propagation and maintains a relatively organised convective structure as the system traverses the Straits of Malacca. In contrast, the uncoupled configuration (cSINGV_A) produces weaker and more fragmented convection, with reduced organisation during its propagation and a diminished signal over Singapore (Fig. 13). These differences suggest that coupling may contribute to sustaining organised convection during its eastward propagation.

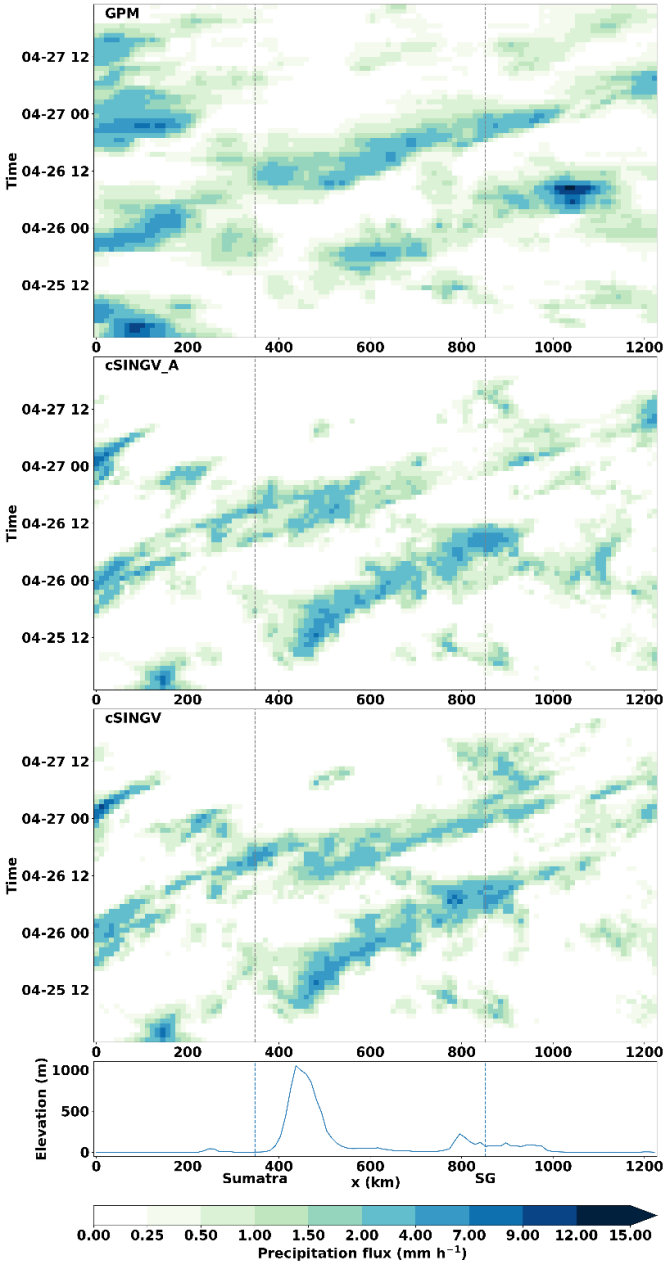


Figure 13: Rotated Hovmöller diagrams of precipitation for the Sumatra squall event (25–27 April 2019) along a transect from Sumatra to Singapore. Top: GPM observations, middle: uncoupled model (cSINGV_A), bottom: coupled model (cSINGV).

To place the 27 April event in a broader context, additional squall cases identified from the MSS database were examined (figures in the Supplement: Fig. S14-16).

The 2–4 April 2019 event (maximum 1 h accumulation of 54 mm) represents a predominantly land-driven case (Fig. S14). Convection initiates over or near the Sumatra mountain region and propagates eastward, with GPM showing relatively coherent structure during the early stages. Both coupled and uncoupled simulations reproduce this evolution with only minor differences, indicating that convection is primarily controlled by land-based processes.

A similar behaviour is observed in the 3–4 September 2019 event (maximum 1 h accumulation of 84 mm), where convection remains broad and fragmented during propagation (Fig. S15). Both model configurations show comparable skill, with only slight improvements in organisation in the coupled simulation. Notably, while significant rainfall over Singapore is recorded in the MSS database, the GPM observations do not clearly capture this signal, whereas both simulations indicate convection reaching the region.

In contrast, the 2–4 November 2020 event (maximum 1 h accumulation of 75.8 mm) exhibits a more organised and continuous convective structure during its eastward propagation, closely resembling the 27 April case. While both simulations capture the eastward movement, the coupled configuration maintains a more coherent and intense convective band as the system approaches Singapore, whereas the uncoupled simulation becomes more fragmented (Fig. S16). This behaviour is consistent with enhanced air–sea interactions in the coupled system, which may support the persistence and intensity of convection over the ocean.

Taken together, these cases suggest that the impact of coupling may depends on the dominant convective regime. When convection is initiated and primarily governed by land-based processes, both coupled and uncoupled configurations perform similarly. In contrast, for more organised systems that originate offshore (west coast of Sumatra), coupling appears to play a more important role, potentially by enhancing surface fluxes and supporting the maintenance of convective structure. This regime-dependent behaviour provides a plausible physical interpretation of the coupling effects identified in this study and links directly to the surface flux analysis presented in the next section. However, given the small number of events and the use of single deterministic realisations, this regime dependence should be regarded as a hypothesis to be tested with a larger sample of events or with ensemble simulations.

4.5 Impact of Coupling on Air–Sea Fluxes

To further investigate the processes underlying the differences between the cSINGV and cSINGV_A simulations, we examine the influence of coupling on surface fluxes, with a focus on latent heat flux (LHF). As discussed in Section 4.4, the largest differences between the two configurations occur during the propagation of organised convection, suggesting an important role for air–sea interactions.

Figure 14 shows the mean difference in LHF between the coupled and uncoupled simulations for January–June 2019. The coupled configuration exhibits enhanced upward fluxes across much of the domain, with localised anomalies exceeding 15 W m^{-2} along the Sumatra–Java coastal regions. These enhancements indicate increased transfer of moisture and energy from the ocean to the atmosphere, supporting convective development and maintenance.

To better understand the underlying mechanisms, the LHF differences are decomposed into two components: (i) a wind-speed contribution (ΔU), and (ii) a moisture-gradient contribution ($\Delta(q_s - q_a)$), where q_s is the saturation specific humidity at the sea surface and q_a is the near-surface atmospheric humidity. The wind-related contribution is relatively modest (approximately ±5 W m^{-2}), whereas the moisture-gradient term exhibits larger amplitudes (up to ±12 W m^{-2}). To examine how the LHF differences relate to changes in SST, near-surface winds and sea-surface roughness, January–June mean differences in LHF, SST, 10 m wind speed and the Charnock parameter between cSINGV and cSINGV_A were compared (Fig. S17). The widespread increase in LHF broadly coincides with warmer SST in cSINGV, whereas the wind-speed differences are smaller and more spatially heterogeneous. This suggests that SST-related changes in the near-surface thermodynamic gradients contribute more consistently to the mean LHF response than changes in wind speed, although the individual contributions cannot be isolated from these spatial patterns alone.

From a process perspective, the increased LHF in cSINGV supplies additional moisture and energy to the lower atmosphere, which may support the organisation and persistence of convection during its propagation. This mechanism is consistent with the case studies presented in Section 4.4. In particular, for the 25–27 April 2019 and 2–4 November 2020 events, cSINGV produced greater LHF over parts of the offshore region and a more sustained propagation of the squall than cSINGV_A. The enhanced LHF was primarily associated with changes in the air–sea humidity gradient, providing a physically plausible mechanism through which the coupled configuration may have contributed to the more sustained convection. In contrast, for land-driven cases such as 2–4 April 2019 and 3–4 September 2019, where convection is primarily initiated over the Sumatra landmass, differences in LHF between the two configurations play a smaller role in shaping the system evolution. This is consistent with the relatively similar behaviour of cSINGV and cSINGV_A in these cases, indicating that the influence of coupling on convection is secondary when land-based forcing dominates. However, a larger event sample or ensemble analysis would be needed to establish this systematically.

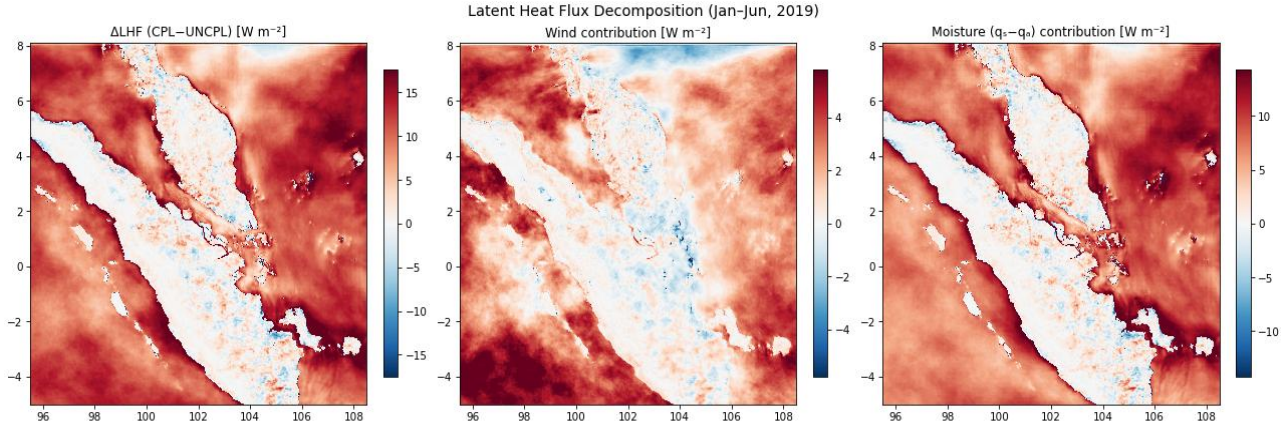


Figure 14: Mean latent heat flux difference (ΔLHF; CPL–UNCPL) over January–June 2019 (left), with decomposition into contributions from surface wind speed (middle) and near-surface humidity gradient (right). Positive values indicate enhanced upward flux in the coupled simulation.

Overall, the coupled configuration provides a more physically consistent representation of key processes in the WMC, including oceanic precipitation, offshore propagation, and air–sea flux interactions. While near-surface atmospheric variables show no systematic improvement and some biases persist for precipitation, particularly over land, the results indicate that atmosphere–ocean–wave coupling can contribute to improved simulation of precipitation characteristics and associated processes in this region.

5 Summary and conclusions

The WMC is characterised by complex interactions between atmospheric convection, ocean variability, and surface wave processes across multiple temporal and spatial scales. Accurately representing these coupled processes remains a major challenge for numerical models, particularly at convection-permitting resolutions.

In this study, a high-resolution (1.5 km) regional coupled atmosphere–ocean–wave modelling system, cSINGV, was developed by integrating the SINGV atmospheric model with newly configured ocean (cSINGV_O) and wave (cSINGV_W) components within the Regional Coupled Suite framework. The system enables two-way interactions between the atmosphere, ocean, and waves, providing a unified platform to investigate air–sea–wave coupling processes in the WMC.

The standalone evaluation of the ocean and wave components demonstrates that both models provide a credible representation of key marine processes. The ocean model shows good agreement with SST observations and reanalysis datasets, while the wave model reproduces the observed variability and distribution of H_s. These results provide confidence in the individual components and establish a credible foundation for the fully coupled system.

The performance of cSINGV was evaluated against an uncoupled atmospheric configuration (cSINGV_A). It should be noted that the uncoupled configuration uses prescribed SST from OSTIA, whereas the coupled system uses dynamically evolving SST from the ocean model. The use of observed SST in the uncoupled simulation provides a realistic surface boundary condition, allowing it to serve as a reference configuration. This facilitates a clearer assessment of the performance of the coupled model relative to the uncoupled baseline.

The results indicate that the coupled configuration influences several key characteristics of precipitation over the WMC. In particular, differences are observed in the spatial organisation of rainfall, the diurnal cycle over the ocean, and the offshore propagation of convection. These effects are most pronounced in oceanic regions, while near-surface atmospheric variables such as wind speed and air temperature show comparatively limited sensitivity to coupling. The FSS analysis indicates a robust improvement in the representation of overall rainfall occurrence, although the improvement for heavier rainfall is smaller and less conclusive. Evaluation of cSINGV against observations also shows credible SST and H_s performance comparable to those of the standalone components.

Process-based analysis suggests that these differences are primarily associated with thermodynamic air–sea feedbacks. Analysis of latent heat flux reveals that the coupled system produces enhanced upward fluxes, primarily driven by increased

air–sea humidity gradients associated with SST variability. This enhanced moisture supply may support the organisation and persistence of convection over the ocean. Case studies of individual Sumatra squall events further suggest that the influence of coupling may depend on the convective regime. For land-driven convection, both coupled and uncoupled configurations show similar behaviour, whereas for convection originating over the ocean, the coupled system produced more organised convective structures and sustained their propagation more effectively than the uncoupled configuration in the cases examined. Because these findings are based on individual events, they should not be interpreted as generally representative of all Sumatra squalls.

Several limitations should be considered when interpreting these results. First, the comparison between cSINGV and cSINGV_A is not a fully controlled experiment. In addition to interactive feedbacks, the configurations differ in SST forcing frequency: OSTIA SST in cSINGV_A is updated daily and remains fixed within each day, whereas SST in cSINGV evolves hourly. The configurations also differ in their treatment of sea-surface roughness, with cSINGV_A using a fixed Charnock parameter and cSINGV using a wave-dependent value. The present experiments therefore cannot separate the effects of interactive coupling from those of sub-daily SST variability and wave-dependent roughness. Additional sensitivity experiments, such as an atmosphere-only simulation forced with hourly SST from cSINGV, would be required to isolate these contributions. Second, the findings are based on single deterministic six-month simulations and therefore do not account for internal atmospheric variability. Differences between the squall simulations, and the inferred dependence on convective regime, should consequently be regarded as indicative rather than conclusive. Third, component parameters, including the WW3 wind-input parameter *betamax*, were selected during standalone model development, while the hourly coupling interval was adopted as a practical design choice. Neither has been demonstrated to be optimal for the fully coupled system.

The computational cost of the present research configuration provides useful context for its potential operational application (Table S5). The fully coupled cSINGV configuration requires approximately twice the allocated core-hours of cSINGV_A. However, the additional resources allow the atmosphere, ocean, and wave components to run concurrently, keeping the wall-clock time close to that of the atmosphere-only simulation, with an increase of only approximately 5%. These timings are specific to the present research configuration and may vary with computing architecture, resource allocation, model configuration, and operational workflow.

Overall, this study demonstrates that high-resolution atmosphere–ocean–wave coupling provides a physically consistent framework for representing air–sea interactions in the WMC and offers a valuable tool for investigating coupled processes in this region.

6 Future developments

River runoff at the ocean model's coastal grid cells is currently prescribed from a climatological dataset rather than supplied interactively by the SINGV–JULES land-surface system. Implementing interactive freshwater exchange between the land and ocean components is therefore an important priority. Ongoing work is focused on improving the representation of river

discharge within the coupled atmosphere–land system, with the aim of enabling fully consistent land–ocean coupling in future versions of cSINGV.

Further development will focus on advancing cSINGV towards an operational environment prediction system through the implementation of coupled data assimilation. This will involve the integration of atmospheric, oceanic, and wave observations to provide dynamically consistent initial conditions across all components of the coupled system.

Future studies will also evaluate of cSINGV across a wider range of meteorological regimes, including monsoon transitions, cold surges, and tropical cyclones. An analysis of a larger sample of Sumatra squall events is ongoing to assess the robustness of the regime-dependent coupling impact identified here. Sensitivity experiments are also planned to examine the effects of coupling frequency, role of remotely generated swell, and the separate contributions of sub-daily SST variability. These developments will support the progression of cSINGV towards a more comprehensive and operational coupled prediction system for MSS.

7 Appendix A

The regional WW3 configuration was developed through standalone sensitivity experiments forced by winds from cSINGV_A. Model performance was evaluated against multi-mission satellite altimeter observations for January 2019, using correlation, bias, RMSE, and SI. January 2019 was selected as it includes Tropical Storm Pabuk and therefore provides a strong-wind case for evaluating wave growth. The first set of experiments examined the ST4 wave-growth parameter *betamax*, which controls the maximum wind-input growth rate and strongly influences the development of wind-generated waves (WW3DG, 2019). One-month simulations were performed using *betamax* values ranging from 1.0 to 2.0 (Table S6). A value of *betamax*=1.75 was found to provide the best agreement with altimeter observations, produced the lowest RMSE (0.24 m) together with a relatively small bias (−0.08 m). For comparison, the values of 1.39 and 1.43 used by the Met Office and ECMWF configurations, respectively, produced a bias of approximately −0.12 m. Based on the overall balance among the evaluation metrics, *betamax* = 1.75 was selected for the subsequent experiments.

With *betamax* fixed at 1.75, a second set of experiments examined different combinations of the shallow-water physics options defined in Table 2.6 of the WW3 manual (WW3DG, 2019). The evaluation statistics are summarized in Table S7. Experiment 10 was selected as the final configuration because it provided the best overall performance across the evaluated metrics. The final wave-growth and swell-dissipation parameters specified in the SIN4 namelist are listed in Table S8; these values are consistent with the configuration of Alday et al. (2022). The selected configuration was established using standalone wave simulations and subsequently held fixed in all coupled experiments; its parameters were not adjusted to improve coupled-model performance.

Code availability

The cSINGV modelling system is based on established community models, including the Met Office Unified Model (UM), the NEMO ocean model (v4.0.4), and WAVEWATCH III (WW3 v7.12), coupled using the OASIS3-MCT coupler within the Regional Coupled Suite (RCS) framework.

The coupled configuration used in this study is based on the RCS suite (suite ID: u-bf945), with a dedicated *cSINGV* branch developed for this application and accessible via the Met Office repository (https://code.metoffice.gov.uk/svn/roses-u/b/f/9/4/5/u-bf945_add_cSINGV_br). This branch provides the workflow and coupling configuration required to reproduce the coupled atmosphere–ocean–wave system presented in this study.

The configuration files, namelists, model grids, ancillary files, forcing datasets, and run scripts required to reproduce the cSINGV v1.0 simulations are archived in a Zenodo repository (DOI: 10.5281/zenodo.21449436). The repository is currently under restricted access because it contains materials associated with third-party software and datasets that are subject to licensing restrictions (Kumar, R. 2026). Access may be granted upon reasonable request to the corresponding author for the purpose of reproducing the results presented in this manuscript, subject to the applicable licence agreements.

The source code of the Unified Model (UM) used in this study is archived on the JASMIN data infrastructure. Instructions for obtaining access to the archived UM source code are provided in the accompanying UM_Source_code.docx file included in the Zenodo repository. Access to the Unified Model source code is subject to the Met Office licensing conditions.

The Joint UK Land Environment Simulator (JULES) is available free of charge under licence. Further information on obtaining access for research purposes is available at http://jules.jchmr.org (last access: 20 January 2025). The JULES vn7.5 trunk code is accessible to registered users via the Met Office JULES code repository (https://code.metoffice.gov.uk/trac/jules/wiki; last access: 20 January 2025).

The NEMO ocean model and WAVEWATCH III are open-source models and can be accessed through their respective repositories following registration (https://www.nemo-ocean.eu/; https://polar.ncep.noaa.gov/waves/wavewatch/wavewatch.shtml).

OASIS3-MCT (version 4.0) is available as open-source software from https://oasis.cerfacs.fr/en/ (last access: 20 March 2026).

Model evaluation of near-surface atmospheric variables was performed using the MetPlus framework (last access: 4 April 2026; https://metplus.readthedocs.io/en/latest/).

The configuration files, namelists, model grids, and post-processing scripts used in this study are available from the corresponding author upon reasonable request.

Data availability

The high-resolution six-month simulations of the atmosphere, ocean, wave, and coupled configurations generate large data volumes and are therefore not publicly archived. These data can be made available from the corresponding author upon reasonable request.

Processed datasets used for the analysis and figure production in this study are publicly available via Zenodo at https://doi.org/10.5281/zenodo.18797904 (Kumar and Alvin, 2026).

The ERA5 reanalysis data used in this study are available from the European Centre for Medium-Range Weather Forecasts (ECMWF) (https://www.ecmwf.int/). Ocean reanalysis data are obtained from the Copernicus Marine Environment Monitoring Service (CMEMS) (https://marine.copernicus.eu/).

Precipitation data from the GPM IMERG product are available from NASA (https://gpm.nasa.gov/), and satellite altimeter data are obtained from CMEMS (https://marine.copernicus.eu/). OSTIA sea surface temperature data are available from the UK Met Office (https://www.metoffice.gov.uk/).

Observational station data from the WMO MetDB database are subject to access restrictions and are not publicly available but can be obtained through appropriate data-sharing agreements.

Author contributions

R.K. developed the coupled modelling system, with support from J.M.C., C.S. and B.T. Ocean model was developed by R.K. Wave model was developed by R.K. and J.L. C.S. and P.P. contributed to the evaluation methodology. R.K., and A.N performed the data analysis. A.N. and K.S contributed to the wave model evaluation. H.Y. and L.J provided system and software support. R.K. performed the simulations and led the manuscript writing, with contributions from K.F., C.S., B.T and H.Z. All authors contributed to the interpretation of results and to the review and editing of the manuscript.

Competing interests

The authors declare that they have no conflict of interest.

Acknowledgements

The author thanks Dr Dale Barker, Director of CCRS, for his support, encouragement, and constructive comments throughout this work. We are also grateful to Segolene Berthou (Met Office) for her support during the development of the coupled system and for valuable scientific and technical discussions on model coupling. We also thank Jeff Polton (National Oceanographic Centre, UK) for insightful suggestions on NEMO model tuning, and V. Prasanna (CCRS) for helpful discussions on model evaluation.

We thank James Bruten and the Momentum Partnership team for facilitating access to the UM source code for review purposes.

We acknowledge the Working Group on Regional Coupled Modelling (Met Office) for valuable technical discussions, and the MONSOON HPC facility for supporting the initial stages of model development and testing. The authors also acknowledge the use of computational resources provided by the HPC CCRS.

We thank ECMWF, CMEMS, and NASA for providing the datasets used in this study.

References

Alday, M., Ardhuin, F., Dodet, G., and Accensi, M.: Accuracy of numerical wave model results: application to the Atlantic coasts of Europe, Ocean Sci., 18, 1665–1689, https://doi.org/10.5194/os-18-1665-2022, 2022.

Aldrian, E., Sein, D., Jacob, D., Gates, L. D., & Podzun, R.: Modelling Indonesian rainfall with a coupled regional model. *Climate Dynamics*, 25(1), 1–17. https://doi.org/10.1007/s00382-004-0483-0, 2005

Ardhuin, F., et al.: Semi-empirical dissipation source functions for ocean waves. Part I: Definition, calibration and validation. Journal of Physical Oceanography, 40(9), 1917–1941, https://doi.org/10.1175/2010JPO4324.1, 2010

Argüeso, D., R. Romero, and V. Homar: Precipitation Features of the Maritime Continent in Parameterized and Explicit Convection Models. *J. Climate*, 33, 2449–2466, https://doi.org/10.1175/JCLI-D-19-0416.1, 2020

Babanin, A. V.: On a wave-induced turbulence and a wave-mixed upper ocean layer. Geohpysical Research Letters, 33 (L20605), https://doi.org/10.1029/2006GL027308, 2006

Best, M. J., Beljaars, A., Polcher, J., and Viterbo, P.: A proposed structure for coupling tiled surfaces with the planetary boundary layer, J. Hydrometeorol., 5, 1271–1278, https://doi.org/10.1175/JHM-382.1, 2004.

Best, M. J., Pryor, M., Clark, D. B., Rooney, G. G., Essery, R. L. H., Ménard, C. B., Edwards, J. M., Hendry, M. A., Porson, A., Gedney, N., Mercado, L. M., Sitch, S., Blyth, E., Boucher, O., Cox, P. M., Grimmond, C. S. B., and Harding, R. J.: The Joint UK Land Environment Simulator (JULES), model description – Part 1: Energy and water fluxes, Geosci. Model Dev., 4, 677–699, https://doi.org/10.5194/gmd-4-677-2011, 2011.

Birch, C. E., S. Webster, S. C. Peatman, D. J. Parker, A. J. Matthews, Y. Li, and M. E. E. Hassim: Scale interactions between the MJO and the western Maritime Continent. J. Climate, 29, 2471–2492, https://doi.org/10.1175/JCLI-D-15-0557.1, 2016

Bonino, G., Iovino, D., Brodeau, L., & Masina, S.: The bulk parameterizations of turbulent air–sea fluxes in NEMO4: The origin of sea surface temperature differences in a global model study. *Geoscientific Model Development, 15*, 6873–6889. https://doi.org/10.5194/gmd-15-6873-2022, 2022

Booij, N. and Holthuijsen, L. H.: Propagation of ocean waves in discrete spectral wave models, J. Comput. Phys., 68, 307–326, https://doi.org/10.1016/0021-9991(87)90060-X, 1987.

Boutle, I.A., Eyre, J.E.J. and Lock, A.P.: Seamless stratocumulus simulation across the turbulent gray zone. *Monthly Weather Review*, 142, 1655–1668. https://doi.org/10.1175/MWR-D-13-00229.1, 2014

Breivik, Ø., K.Mogensen, J.-R.Bidlot, M. A.Balmaseda, and P. A. E. M.Janssen: Surface wave effects in the NEMO ocean model: Forced and coupled experiments, J. Geophys. Res. Oceans, 120, 2973–2992, doi:10.1002/2014JC010565, 2015

Bruciaferri, D., Tonani, M., Lewis, H. W., Siddorn, J. R., Saulter, A., Castillo, J. M., et al.: The impact of ocean-wave coupling on the upper ocean circulation during storm events. Journal of Geophysical Research: Oceans, 126(6), e2021JC017343. https://doi.org/10.1029/2021JC017343, 2021

Bush, M. et al.: The second Met Office Unified Model–JULES Regional Atmosphere and Land configuration, RAL2. *Geosci. Model. Dev.* 16, 1713–1734, https://doi.org/10.5194/gmd-16-1713-2023, 2023.

Lyard, F. H., Allain, D. J., Cancet, M., Carrère, L., and Picot, N.: FES2014 global ocean tide atlas: design and performance, Ocean Sci., 17, 615–649, https://doi.org/10.5194/os-17-615-2021, 2021.

Castillo, J. M., et al.: The Regional Coupled Suite (RCS-IND1): application of a flexible regional coupled modelling framework to the Indian region at kilometre scale, Geosci. Model Dev., 15, 4193–4223, https://doi.org/10.5194/gmd-15-4193-2022, 2022.

Cavaleri, L., Fox-Kemper, B., and Hemer, M.: Wind waves in the coupled climate system, B. Am. Meteorol. Soc., 93, 1651–1661, https://doi.org/10.1175/BAMS-D-11-00170.1, 2012.

Craig, A., Valcke, S., and Coquart, L.: Development and performance of a new version of the OASIS coupler, OASIS3-MCT_3.0, Geosci. Model Dev., 10, 3297–3308, https://doi.org/10.5194/gmd-10-3297-2017, 2017.

Dai, A., & Trenberth, K. E.: Estimates of freshwater discharge from continents: Latitudinal and seasonal variations. Journal of Hydrometeorology, 3(6), 660-687, https://doi.org/10.1175/1525-7541(2002)003<0660:EOFDFC>2.0.CO;2, 2002

DaSilva, N. A., Webber, B. G. M., Matthews, A. J., Feist, M. M., Stein, T. H. M., Holloway, C. E., & Abdullah, M. F. A. B.: Validation of GPM IMERG extreme precipitation in the Maritime Continent by station and radar data. Earth and Space Science, 8, e2021EA001738. https://doi.org/10.1029/2021EA001738, 2021

Davies, H.: A lateral boundary formulation for multi-level prediction models, Q. J. Roy. Meteor. Soc., 102, 405–418, https://doi.org/10.1002/qj.49710243210, 1976.

DeMott, C. A., Klingaman, N. P., & Woolnough, S. J.: Atmosphere-ocean coupled processes in the Madden-Julian oscillation. *Reviews of Geophysics, 53*, 1099–1154. https://doi.org/10.1002/2014RG000478, 2015

Dipankar, A., S. Webster, X. Huang, and V. Q. Doan: Understanding Biases in Simulating the Diurnal Cycle of Convection over the Western Coast of Sumatra: Comparison with Pre-YMC Observation Campaign. *Mon. Wea. Rev.*, 147, 1615–1631, https://doi.org/10.1175/MWR-D-18-0432.1, 2019

Donlon, C. J., Martin, M., Stark, J., et al.: The Operational Sea Surface Temperature and Sea Ice Analysis (OSTIA) system. Remote Sensing of Environment, 116, 140-158, https://doi.org/10.1016/j.rse.2010.10.017, 2012

Edwards, J.M. and Slingo, A.: Studies with a flexible new radiation code. I: Choosing a configuration for a large-scale model. *Quarterly Journal of the Royal Meteorological Society*, 122(531), 689–719. https://doi.org/10.1002/qj.49712253107, 1996

Flather, R. A.: A tidal model of the northeast pacific. *Atmosphere-Ocean*, *25*(1), 22–45. https://doi.org/10.1080/07055900.1987.9649262, 1987.

Hasselmann, K., et al.: Measurements of wind-wave growth and swell decay during the joint North Sea wave project (JONSWAP), Erg"anzungsheft Reihe A; Deutsche Hydrographische Zeitschrift: Hamburg, Germany, Volume 12, p. 75. [Google Scholar],1973.

Hasselmann, S., Hasselmann, K., Allender, J. H., and Barnett, T. P.: Computations and Parameterizations of the Nonlinear Energy Transfer in a Gravity-Wave Specturm. Part II: Parameterizations of the Nonlinear Energy Transfer for Application in Wave Models, J. Phys. Oceanogr., 15, 1378–1391, https://doi.org/10.1175/1520-0485(1985)015<1378:CAPOTN>2.0.CO;2, 1985.

Heng, B.C.P., Tubbs, R.N., Huang, X.-Y., Macpherson, B., Barker, D.M., Boyd, D.F.A., Kelly, G., NorthL Stewart, R., Webster, S. and Wlasak, M.: SINGV-DA: a data assimilation system for convective-scale numerical weather prediction over Singapore. *Quarterly Journal of the Royal Meteorological Society*, 146(729), 1923–1938. https://doi.org/10.1002/qj.3774, 2020

Hersbach, H., Bell, B., Berrisford, P., et al.: The ERA5 global reanalysis. Quarterly Journal of the Royal Meteorological Society, 146(730), 1999-2049, https://doi.org/10.1002/qj.3803, 2020.

Hilmi I, Ningsih NS, Sofian I, Hanifah F, Rizal AM.: The study of MJO impact on wave height and wind speed in Indonesian Seas. IOP Conf Ser Earth Environ Sci 162:012004. https://doi.org/10.1088/1755-1315/162/1/012004, 2018.

Howard, E., Woolnough, S., Klingaman, N., Shipley, D., Sanchez, C., Peatman, S. C., Birch, C. E., & Matthews, A. J.: Evaluation of multi-season convection-permitting atmosphere–mixed-layer ocean simulations of the Maritime Continent. *Geoscientific Model Development, 17*, 3815–3837. https://doi.org/10.5194/gmd-17-3815-2024, 2024.

Huang, X.-Y., Barker, D., Webster, S., Dipankar, A., Lock, A., Mittermaier, M., Sun, X. M., North, R., Darvell, R., Boyd, D., Lo, J., Liu, J. Y., Macpherson, B., Heng, P., Maycock, A., Pitcher, L., Tubbs, R., McMillan, M., Zhang, S. J., Hagelin, S., Porson, A., Song, G. T., Beckett, B., Cheong, W. K., Semple, A., and Gordon, C.: SINGV – the convective-scale numerical weather prediction system for Singapore, ASEAN J. Sci. Tech. Dev., 36, 81–90, https://doi.org/10.29037/ajstd.581, 2019.

Huffman, G. J., Stocker, E. F., Bolvin, D. T., Nelkin, E. J., & Tan, J.: *GPM IMERG final precipitation L3 half hourly 0.1 degree×0.1 degree V06*. Goddard Earth Sciences Data and Information Services Center (GES DISC). https://doi.org/10.5067/GPM/IMERG/3B-HH/06, 2019

Ikuyajolu, O. J., Van Roekel, L., Brus, S. R., Thomas, E. E., Deng, Y., & Benedict, J. J.: Effects of surface turbulence flux parameterizations on the MJO: The role of ocean surface waves. *Journal of Climate, 37*, 3011–3036. https://doi.org/10.1175/JCLI-D-23-0490.1, 2024.

Itterly, K., Taylor, P., & Roberts, J. B.: Satellite perspectives of sea surface temperature diurnal warming on atmospheric moistening and radiative heating during MJO. *Journal of Climate, 34*, 1203–1226, https://doi.org/10.1175/JCLI-D-20-0350.1, 2021.

Jiang, X., and Coauthors.: Fifty years of research on the Madden-Julian Oscillation: Recent progress, challenges, and perspectives. *Journal of Geophysical Research: Atmospheres, 125*, e2019JD030911. https://doi.org/10.1029/2019JD030911, 2020.

Jiang, L., Li, T.: Why rainfall response to El Niño over Maritime Continent is weaker and non-uniform in boreal winter than in boreal summer. *Clim Dyn* 51, 1465–1483. https://doi.org/10.1007/s00382-017-3965-6, 2018.

Jing, Y., Sun, J., Li, R., Wu, K., Yu, Z., Lin, P., Dong, X., & Babanin, A. V.: *The impact of wave-induced mixing on the simulation of the upper mixed layer in climate models*. Ocean Modelling, *197*, 102583. https://doi.org/10.1016/j.ocemod.2025.102583, 2025.

Karlowska, E., Matthews, A. J., Webber, B. G. M., Graham, T., & Xavier, P.: Two-way feedback between the Madden–Julian Oscillation and diurnal warm layers in a coupled ocean–atmosphere model. *Quarterly Journal of the Royal Meteorological Society, 150*(764), 4113–4132. https://doi.org/10.1002/qj.4807, 2024a.

Karlowska, E., Matthews, A. J., Webber, B. G. M., Graham, T., & Xavier, P.: The effect of diurnal warming of sea-surface temperatures on the propagation speed of the Madden–Julian oscillation. *Quarterly Journal of the Royal Meteorological Society, 150*, 334–354, https://doi.org/10.1002/qj.4599, 2024b.

Kim, H.-R., Ha, K.-J., Moon, S., Oh, H., & Sharma, S.: Impact of the Indo-Pacific warm pool on the Hadley, Walker, and monsoon circulations. *Atmosphere, 11*, 1030, https://doi.org/10.3390/atmos11101030, 2020.

Kumar, R., & Alvin, N. Z. H.: Supporting data: Evaluation of the cSINGV v1.0 coupled atmosphere-ocean-wave modelling system for the Western Maritime Continent. Zenodo. https://doi.org/10.5281/zenodo.18797904, 2026.

Kumar, R. (2026). Model Configuration, Namelists, and Forcing Data for the cSINGV Coupled Regional Modelling System [Dataset]. Zenodo. https://doi.org/10.5281/zenodo.21449437

Kumar, R., Lemos, G., Semedo, Á., & Li, J.-G.: A global high-resolution CMIP6 ensemble of wave climate simulations and projections using a coastal multigrid: Configuration and performance evaluation. *Ocean Modelling*, 197, 102566. https://doi.org/10.1016/j.ocemod.2025.102566, 2025.

Lan, Y.-Y., Hsu, H.-H., & Tseng, W.-L.: Quantifying the impact of SST feedback frequency on Madden–Julian oscillation simulations. *Geoscientific Model Development, 17*, 3897–3918. https://doi.org/10.5194/gmd-17-3897-2024, 2024.

Lau, N.-C., & Nath, M. J.: Atmosphere-ocean variations in the Indo-Pacific sector during ENSO episodes. *Journal of Climate, 16*, 3–20, https://doi.org/10.1175/1520-0442(2003)016<0003:AOVITI>2.0.CO;2, 2003.

Lellouche, J.-M., et al.: The Copernicus Global ° Oceanic and Sea Ice GLORYS12 Reanalysis, Front. Earth Sci., 9, 1–27, https://doi.org/10.3389/feart.2021.698876, 2021.

Li, J. G.: Upstream nonoscillatory advection schemes, Mon. Weather Rev., 136, 4709–4729, https://doi.org/10.1175/2008MWR2451.1, 2008.

Li, J.G.: Propagation of ocean surface waves on a spherical multiple-cell grid. J. Comput. Phys., 231, 8262-8277. doi: 10.1016/j.jcp.2012.08.007, 2012.

Li, J.-G.: An efficient multi-resolution grid for global models and coupled systems. Adv. Sci. Res. 16, 137–142. https://doi.org/10.5194/asr-16-137-2019, 2019.

Li, Y., Jourdain, N. C., Taschetto, A. S., Gupta, A. S., Argüeso, D., Masson, S., and Cai, W.: Resolution dependence of the simulated precipitation and diurnal cycle over the Maritime Continent, Clim. Dynam., 48, 4009–4028, https://doi.org/10.1007/s00382-016-3317-y, 2017.

Lilly, D.K.: On the numerical simulation of buoyant convection. *Tellus*, 14(2), 148–172, https://doi.org/10.3402/tellusa.v14i2.9537, 1962.

Lo, J. C.-F., and Orton, T.: The general features of tropical Sumatra squalls, *Weather*, 71, 173–178, https://doi.org/10.1002/wea.2748, 2016.

Lock, A.P., Brown, A.R., Bush, M.R., Martin, G.M. and Smith, R.N.B.: A new boundary layer mixing scheme. Part I: Scheme description and single-column model tests. *Monthly Weather Review*, 128, 3187-3199, https://doi.org/10.1175/1520-0493(2000)128<3187:ANBLMS>2.0.CO;2, 2000.

Madec, G., et al.: NEMO ocean engine, in: Notes du Pôle de modélisation de l'Institut Pierre-Simon Laplace (IPSL), Zenodo, https://doi.org/10.5281/zenodo.3248739, 2017.

Makrygianni, N., Berthou, S., Flack, D. L. A., Lebeaupin Brossier, C., Beuvier, J., Castillo, J. M., Renzi, E., O'Neill, C., Peláez-Zapata, D., Dias, F., Lewis, H., and Bruciaferri, D.: Representation of meteotsunamis in km-scale regional simulations coupled at high frequency, *Nat. Hazards Earth Syst. Sci.*, 26, 3185–3211, https://doi.org/10.5194/nhess-26-3185-2026, 2026.

Manners, J., Vosper, S. B., and Roberts, N.: Radiative transfer over resolved topographic features for high-resolution weather prediction, Q. J. Roy. Meteor. Soc., 138, 720–733, https://doi.org/10.1002/qj.956, 2012.

Massey Jr., F.J., 1951. The Kolmogorov–Smirnov test for goodness of fit. J. Am. Stat. Assoc. 46 (253), 68–78. https://doi.org/10.1080/01621459.1951.10500769.

Met Office.: LAND SYNOP reports from land stations collected by the Met Office MetDB System. NCAS British Atmospheric Data Centre, https://catalogue.ceda.ac.uk/uuid/9f80d42106ba708f92ada730ba321831/, (*last accessed December 2024*), 2008.

Mori, S., and Coauthors*:* Diurnal land–sea rainfall peak migration over Sumatera Island, Indonesian Maritime Continent, observed by TRMM satellite and intensive rawinsonde soundings. *Mon. Wea. Rev.*, *132*, 2021–2039, doi:10.1175/1520-0493(2004)132<2021:DLRPMO>2.0.CO;2., 2004.

Neale, R. B., & Slingo, J. M.: The Maritime Continent and its role in the global climate: A GCM study. Journal of Climate, 16(5), 834–848, https://doi.org/10.1175/1520-0442(2003)016<0834:TMCAIR>2.0.CO;2, 2003.

NEMO development team: NEMO ocean model, NEMO ocean engine. In Notes du Pôle de modélisation de l'Institut Pierre-Simon Laplace (IPSL) (Version v4.0, Issue 27), Zenodo. https://doi.org/10.5281/zenodo.3878122, 2021.

Hooker, S. B. and McClain, C. R.: The calibration and validation of SeaWiFS data, Prog. Oceanogr., 45, 427–465, https://doi.org/10.1016/S0079-6611(00)00012-4, 2000.

OASIS3-MCT development team: OASIS3-MCT coupling libraries, CERFACS / oasis3-mct · GitLab (last access: 20 March 2026), 2022.

Odland, T.: tommyod/KDEpy: Kernel Density Estimation in Python (v0.9.10). Zenodo. https://doi.org/10.5281/zenodo.2392268, 2018.

Oliver et al., "Workflow Automation for Cycling Systems: The Cylc Workflow Engine", Computing in Science & Engineering Vol 21, Issue 4, July/Aug 2019. DOI: 10.1109/MCSE.2019.2906593, 2019.

Parzen, E.: On Estimation of a Probability Density Function and Mode. *The Annals of Mathematical Statistics*, *33*(3), 1065–1076, https://doi.org/10.1214/aoms/1177704472, 1962.

Peatman, S. C., Matthews, A. J., & Stevens, D. P.: Propagation of the Madden–Julian Oscillation through the Maritime Continent and scale interaction with the diurnal cycle of precipitation. *Quarterly Journal of the Royal Meteorological Society, 140*(680), 814–825, https://doi.org/10.1002/qj.2161, 2014.

Peatman, S. C., et al.: A local-to-large scale view of Maritime Continent rainfall: control by ENSO, MJO, and equatorial waves. J Clim 34(22):8933–8953, https://doi.org/10.1175/JCLI-D-21-0263.1, 2021.

Peatman, S. C., Birch, C. E., Schwendike, J., Marsham, J. H., Howard, E., Woolnough, S. J., Mustafa, J. M., & Matthews, A. J.: Physical controls on the variability of offshore propagation of convection from Sumatra. *Journal of Geophysical Research: Atmospheres*, *130*(7), Article e2024JD042458. https://doi.org/10.1029/2024JD042458, 2025.

Prasanna, V., Dipankar, A., Liu, J., Lim, G., et al.: Evaluating SINGV-RCM for long-term high-resolution climate simulations over Southeast Asia, *Int. J. Climatol.*, 45, no. 11, e8932, https://doi.org/10.1002/joc.8932, 2025.

Piollé, J.-F.; Dodet, G.; Quilfen, Y.: ESA Sea State Climate Change Initiative (Sea_State_cci): Global remote sensing daily merged multi-mission along-track significant wave height from altimetry, L3 product, version 3. NERC EDS Centre for Environmental Data Analysis, *11 October 2022*. doi:10.5285/e6af67fca81c40b7bb3eddaadde06909 (last accessed 20 March 2026), 2022.

Roberts, N. M., & Lean, H. W.: Scale-selective verification of rainfall accumulations from high-resolution forecasts of convective events. Monthly Weather Review, 136(1), 78-97, https://doi.org/10.1175/2007MWR2123.1, 2008.

Ruppert, J. H., & Johnson, R. H.: Diurnally modulated cumulus moistening in the preonset stage of the Madden–Julian oscillation during DYNAMO. *Journal of the Atmospheric Sciences, 72*(4), 1622–1647, https://doi.org/10.1175/JAS-D-14-0218.1, 2015.

Rutgersson, A., E. O.Nilsson, and R.Kumar.: Introducing surface waves in a coupled wave-atmosphere regional climate model: Impact on atmospheric mixing length, J. Geophys. Res., 117, C00J15, doi:10.1029/2012JC007940, 2012.

Savarin, A., & Chen, S. S.: Pathways to better prediction of the MJO: 2. Impacts of atmosphere–ocean coupling on the upper ocean and MJO propagation. *Journal of Advances in Modeling Earth Systems, 14*, e2021MS002929. https://doi.org/10.1029/2021MS002929, 2022.

Senior, N.V., Matthews, A.J., Webber, B.G.M., Paski, J.A.I., Nuryanto, D.E., Jones, R.W., et al.: Abrupt ending of the Madden–Julian Oscillation by convectively coupled Kelvin wave precipitation leaves a swath of flooding across Indonesia. Quarterly Journal of the Royal Meteorological Society, 151(771), e4997. Available from: https://doi.org/10.1002/qj.4997, 2025.

Seo, H., Subramanian, A. C., Miller, A. J., & Cavanaugh, N. R.: Coupled impacts of the diurnal cycle of sea surface temperature on the Madden–Julian Oscillation. *Journal of Climate, 27*, 8422–8443, https://doi.org/10.1175/JCLI-D-14-00141.1, 2014.

Siddorn, J. R. and Furner, R.: An analytical stretching function that combines the best attributes of geopotential and terrain-following vertical coordinates, Ocean. Model., 66, 1–3, https://doi.org/10.1016/j.ocemod.2013.02.001, 2013.

Stone, P. H., & Chervin, R. M.: The influence of ocean surface temperature gradient and continentality on the Walker circulation. Part II: Prescribed global changes. *Monthly Weather Review, 112*, 1524-1534, https://doi.org/10.1175/1520-0493(1984)112<1524:TIOOST>2.0.CO;2, 1984.

Thompson, B., Sanchez, C., Heng, B. C. P., Kumar, R., Liu, J., Huang, X.-Y., and Tkalich, P.: Development of a MetUM (v 11.1) and NEMO (v 3.6) coupled operational forecast model for the Maritime Continent – Part 1: Evaluation of ocean forecasts, Geosci. Model Dev., 14, 1081–1100, https://doi.org/10.5194/gmd-14-1081-2021, 2021.

Tolman, H. L.: User manual and system documentation of WAVEWATCH III® version 4.18, http://polar.ncep.noaa.gov/waves/wavewatch/manual.v4.18.pdf, https://polar.ncep.noaa.gov/waves/wavewatch/#subtab2-2, 2014.

Umlauf, L. and Burchard, H.: A generic length-scale equation for geophysical turbulence models, J. Mar. Res., 61, 235–265, https://elischolar.library.yale.edu/journal_of_marine_research/9, 2003.

Wang, P., J. C. McWilliams, D. Wang, and D. L. Yi, 2022: Conservative Surface Wave Effects on a Wind-Driven Coastal Upwelling System. J. Phys. Oceanogr., 53, 37–55, https://doi.org/10.1175/JPO-D-22-0120.1

Wei, J., P. Malanotte-Rizzoli, E. Eltahir, P. Xue, D. Zhang, and D. Xu.: Coupling of a regional atmospheric model (RegCM3) and a regional oceanic model (FVCOM) over the Maritime Continent, Clim. Dyn., 43(5–6), 1575–1594, doi:10.1007/s00382-013-1986-3, 2014.

Wei, Y., Pu, Z., and Zhang, C.: Diurnal Cycle of Precipitation Over the Maritime Continent Under Modulation of MJO: Perspectives From Cloud-Permitting Scale Simulations, J. Geophys. Res.-Atmos., 125, e2020JD032529, https://doi.org/10.1029/2020JD032529, 2020.

Wilson, D.R. and Ballard, S.P.: A microphysically based precipitation scheme for the UK Meteorological Office Unified Model. *Quarterly Journal of the Royal Meteorological Society*, 125(557), 1607–1636. https://doi.org/10.1002/qj.49712555707, 1999.

Wilson, D.R., Bushell, A.C., Kerr-Munslow, A.M., Price, J.D. and Morcrette, C.J.: PC2: a prognostic cloud fraction and condensation scheme. I: Scheme description. *Quarterly Journal of the Royal Meteorological Society*, 134(637), 2093–2107. https://doi.org/10.1002/qj.333, 2008.

WW3DG (The WAVEWATCH III® Development Group): User manual and system documentation of WAVEWATCH III® version 6.07, Tech. Note 333, NOAA/NWS/NCEP/MMAB, College Park, MD, USA, https://github.com/NOAA-EMC/WW3/wiki/Manual, 2019.

Wu, L., Breivik, O., & Rutgersson, A.: Ocean-wave-atmosphere interaction processes in a fully coupled modeling system. Journal of Advances in Modeling Earth Systems, 11, 3852–3874. https://doi.org/10.1029/2019MS001761, 2019.

Xue, P., P. Malanotte-Rizzoli, J. Wei, and E. A. Eltahir: Coupled ocean-atmosphere modeling over the Maritime Continent: A review. Journal of Geophysical Research: Oceans, Vol. 125, No. 6, e2019JC014978. https://doi.org/10.1029/2019JC014978, 2020.

Yamanaka, M. D.: *Physical climatology of Indonesian maritime continent: An outline to comprehend observational studies*. Atmospheric Research, 178–179, 231–259. https://doi.org/10.1016/j.atmosres.2016.03.017, 2016.

Yan, Y., Zhang, L., Yu, Y., Chen, C., Xi, J., & Chai, F.: Rectification of the intraseasonal SST variability by the diurnal cycle of SST revealed by the Global Tropical Moored Buoy Array. *Geophysical Research Letters, 48*, e2020GL090913, https://doi.org/10.1029/2020GL090913, 2021.

Yokoi, S., S. Mori, M. Katsumata, B. Geng, K. Yasunaga, F. Syamsudin, Nurhayati, and K. Yoneyama: Diurnal cycle of precipitation observed in the western coastal area of Sumatra Island: Offshore preconditioning by gravity waves. Mon. Wea. Rev., 145, 3745–3761, https://doi.org/10.1175/MWR-D-16-0468.1, 2017.

Yoneyama, K., & Zhang, C.: Years of the Maritime Continent. *Geophysical Research Letters, 47*, e2020GL087182. https://doi.org/10.1029/2020GL087182, 2020.

Zhao, N., & Nasuno, T.: How does the air-sea coupling frequency affect convection during the MJO passage? *Journal of Advances in Modeling Earth Systems, 12*, e2020MS002058. https://doi.org/10.1029/2020MS002058, 2020.

Zhang, C.: *Madden–Julian Oscillation*. Reviews of Geophysics, 43(2). https://doi.org/10.1029/2004RG000158, 2005.